Jacobian-based Causal Discovery with Nonlinear ICA

Anonymous authors
Paper under double-blind review

Abstract

Today's methods for uncovering causal relationships from observational data either constrain functional assignments (linearity/additive noise assumptions) or the data generating process (e.g., non–i.i.d. assumptions). Unlike previous works, which use conditional independence tests, we rely on the inference function's Jacobian to determine nonlinear cause-effect relationships. We prove that, under strong identifiability, the inference function's Jacobian captures the sparsity structure of the causal graph; thus, generalizing the classic LiNGAM method to the nonlinear case. We use nonlinear Independent Component Analysis (ICA) to infer the underlying sources from the observed variables and show how nonlinear ICA is compatible with causal discovery via non–i.i.d. data. Our approach avoids the cost of exponentially many independence tests and makes our method end-to-end differentiable. We demonstrate that the proposed method can infer the causal graph on multiple synthetic data sets, and in most scenarios outperforms previous work.

1 Introduction

Traditional statistical learning methods model correlations in data. Though they have achieved super-human performance in multiple fields, they have limited value in understanding cause-effect relationships. A prevalent consequence of this shortcoming is the models' tendency to learn from spurious features or shortcuts (Geirhos et al., 2020) (e.g., classifying objects based on their backgrounds). In contrast, *causal models* construct the world according to the Independent Causal Mechanisms (ICM) principle (Peters et al., 2017), where building blocks (mechanisms) neither influence nor inform each other. Modeling temperature T and altitude A is a classic example (Peters et al., 2017): changing A affects T, but not vice versa—this relationship is described by the Directed Acyclic Graph (DAG) $A \to T$. The ICM principle means that the same mechanism $p(T|A)$ describes how altitude affects temperature for different $p(A)$, but the same cannot be said about $p(A|T)$ and $p(T)$.
Causal Discovery (CD) describes the process of extracting causal structure from data in the form of a DAG. Having *interventional* data—such as in the form of Randomized Controlled Trials (RCTs)—is desirable as it enables answering questions of interventional nature, such as 'What will happen if variable X is changed?' However, RCTs can be costly, infeasible (Eberhardt et al., 2005), or even unethical. Thus, developing effective CD methods reliant on *observational* data alone is of significant interest. In general, inferring the causal direction is provably impossible without additional constraints or assumptions (Zhang et al., 2015); therefore, existing methods constrain either the model class (i.e., the functions generating the observations) or the data distribution. On the model side, these constraints include linear (Shimizu et al., 2006; Tashiro et al., 2014; Shahbazinia et al., 2021; Zheng et al., 2018) or specific nonlinear relationships (e.g., with additive noise) (Hoyer et al., 2008; Peters et al., 2011; Schölkopf et al., 2021; Yu et al., 2019; Shen et al., 2022; Lachapelle et al., 2020; Ng et al., 2022). On the data side, assumptions include non-stationarity (Hyvärinen & Morioka, 2016; Monti et al., 2019) or exchangeability (Guo et al., 2022).
CD aims to infer the ground-truth cause-effect relationships, which connects it to the *identifiability* literature, where the goal is to learn a model equivalent to the ground truth (up to indeterminacies, such as permutations or element-wise nonlinearities).
An extensively studied method for learning identifiable representations is Independent Component Analysis (ICA) (Comon, 1994; Hyvärinen et al., 2001), which requires that the inferred components *(sources)* are independent. Recent work has relied on nonlinear Independent Component Analysis (NLICA) for identifiability (Zimmermann et al., 2021; Klindt et al., 2021; Hyvärinen & Morioka, 2016; Willetts & Paige, 2021; Khemakhem et al., 2020a; Hyvärinen et al., 2019; Morioka et al., 2021; Monti et al., 2019; Khemakhem et al.,

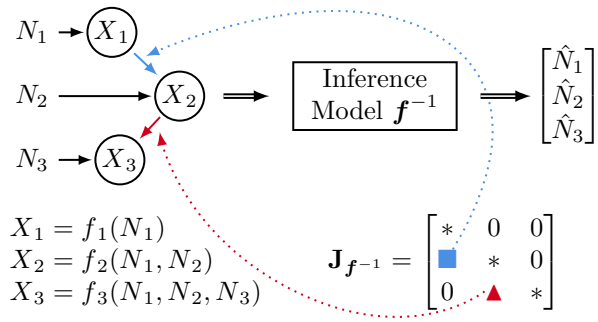

Figure 1: **The Jacobian of the inference network $\mathbf{J}_{\boldsymbol{f}^{-1}}$ informs about the DAG**. We show that if observations $\boldsymbol{X}$ are generated from noise variables $\boldsymbol{N}$ via a general nonlinear Structural Equation Model (SEM) $\boldsymbol{f}$, then the corresponding DAG can be inferred from the Jacobian of a model that identifies $\boldsymbol{N}$ under certain assumptions on $\boldsymbol{N}$

2020b; Gresele et al., 2019; Hyvärinen & Morioka, 2017; Hyvärinen et al., 2010; Hälvä & Hyvärinen, 2020; Lachapelle et al., 2022).

Instead of using pairwise independence tests, we draw inspiration from the Linear Non-Gaussian Acyclic Model (LiNGAM) (Shimizu et al., 2006), which uses a weight matrix to infer the DAG of a linear causal model. We extend this approach to the nonlinear case by showing that the Jacobian of the *ground-truth* inverse Data Generating Process (DGP) (mapping from observations $\boldsymbol{X}$ to noise variables $\boldsymbol{N}$) captures the sparsity structure of the DAG (Prop. 1). Since the ground truth model is generally unknown, we transfer our insight to the Jacobian of the learned *inference model*[1] (i.e., the empirical estimate of the ground-truth $\boldsymbol{X} \to \boldsymbol{N}$ map; cf. Prop. 2). There, we quantify the requirements on the inference model with the notion of strong identifiability is fulfilled (Khemakhem et al., 2020b, Def. 2) (cf. Defn. B.1) and show that causal models provide an inductive bias to resolve the permutation indeterminacy (Lem. 1). We guarantee identifiability via NLICA; thus, our work is akin to the NonSENS method (Monti et al., 2019), which showed that NLICA can be used for bivariate CD with general nonlinear functions and non–i.i.d. observational data. However, our proposal works in the multivariable case. Relying on the Jacobian removes the cost of d^2 independence tests for a DAG with d nodes. However, with current NLICA methods, we could only scale up to ten nodes.

Our **contributions** can be summarized as follows:

1. We prove that the inverse DGP's Jacobian encodes the DAG structure (Prop. 1);
2. We show that causal models allow us to resolve the permutation indeterminacy of ICA (Lem. 1);
3. Our **main result** (Prop. 2) proves that we can infer the DAG from the Jacobian of the inference function, while removing the need for independence tests;
4. We propose an end-to-end multivariable CD method for nonlinear functions from observational but non–i.i.d. data and show how contrastive NLICA is compatible with CD;
5. We experimentally show that our proposed method can infer the DAG across multiple synthetic data sets.

2 Background

Here, we describe causal models and connect their estimation to ICA and defer the details to Appx. A.

Structural Equation Models (SEMs). Given d-dimensional observed $\boldsymbol{X}=(X_1, \ldots, X_d)$ and noise (independent) variables $\boldsymbol{N}=(N_1, \ldots, N_d)$, their causal relationship is given by d *deterministic* functional assignments (Pearl, 2009), constituting the generative model:

$$X_i := f_i\left(\boldsymbol{Pa}_i, N_i\right) \qquad \forall i, \tag{1}$$

[1]In our paper, inference refers only to this process and not to amortized inference for direct graph discovery as proposed in Lorch et al. (2022)

where $\boldsymbol{Pa}_i \subset \boldsymbol{X}$ are the parents of X_i and f_i are the components of the vector-valued function $\boldsymbol{f}$. We describe the computation of $\boldsymbol{X}$ for a given $\boldsymbol{N}$ with an iterative process (denoting the iteration step with a superscript), which is a useful concept for justifying our proposal (§ 3). Initially, $\boldsymbol{N}$ is drawn from its density. To calculate $\boldsymbol{X}$ for $\boldsymbol{N}$, the functional assignment $\boldsymbol{f}$ needs to be applied d times. Namely, according to (1), each X_i requires that its parents $\boldsymbol{Pa}_i$ are calculated. After sampling $\boldsymbol{N}$, only the (empty) parent sets of root nodes are calculated. Thus, the first application of $\boldsymbol{f}$ yields the X_i values for such nodes. In the second iteration, the children of root nodes can be calculated (since we have all parents from the first iteration), and so on. This yields an iterative algorithmic formulation of the SEM, describing the computational graph given by the DAG as:

$$\boldsymbol{X} = \boldsymbol{X}^d := \boldsymbol{f}^{(d)}\left(\boldsymbol{X}^0, \boldsymbol{N}\right) = \boldsymbol{f}\left(\boldsymbol{X}^{(d-1)}, \boldsymbol{N}\right) = \boldsymbol{f}\left(\boldsymbol{f}\ldots\left(\boldsymbol{f}\left(\boldsymbol{X}^0, \boldsymbol{N}\right), \boldsymbol{N}\right), \boldsymbol{N}\right), \tag{2}$$

where $\boldsymbol{X}^0$ is the initial value (w.l.o.g., we assume $\boldsymbol{X}^0 = \boldsymbol{0}$, since calculating the functional assignments will overwrite every X_i). We will also denote $\boldsymbol{X} = \boldsymbol{X}(\boldsymbol{N})$ to indicate that $\boldsymbol{X}$ is *deterministically* determined by a particular $\boldsymbol{N}$. As in most previous works (Vowels et al., 2022, Table 1), we assume *no confounders* (all variables are observed) and *faithfulness* (loosely speaking, the coefficients/functions will not cancel an edge, cf. Assum. 1).

Causal Discovery (CD). In CD, the data is assumed to be generated by a causal process, and the aim is to infer the corresponding DAG, which enables reasoning about interventions (without the DAG, the joint distribution $p(\boldsymbol{N})$ only admits observational queries) (Peters et al., 2017; Pearl, 2009). Algorithmic approaches include combinatoric search (Shimizu et al., 2006; Hoyer et al., 2008; Hyttinen et al., 2013; Mitrovic et al., 2018; Raskutti & Uhler, 2018; Spirtes et al., 2000; Vowels et al., 2022), continuous optimization (Zheng et al., 2018; Lee et al., 2019; Wei et al., 2020; Ng et al., 2020; Vowels et al., 2022), and neural networks (Yu et al., 2019; Ng et al., 2022; Khemakhem et al., 2021; Yang et al., 2021; Goudet et al., 2018; Kalainathan et al., 2018; Vowels et al., 2022; Kyono et al., 2020; Moraffah et al., 2020)—we focus on the latter. Zhang et al. (2015) proved that identifying the causal direction in a general SEM is impossible without constraints on the function class and/or data distribution.
Functional constraints can include linear (Shimizu et al., 2006; Zheng et al., 2018; Squires et al., 2023), additive nonlinear ($X_i = f_i(\boldsymbol{Pa}_i) + N_i$) (Hoyer et al., 2008; Ng et al., 2022; Lachapelle et al., 2020; Schölkopf et al., 2021; Yang et al., 2021), or affine nonlinear ($X_i = f_i(\boldsymbol{Pa}_i) + h_i(N_i)$) (Khemakhem et al., 2021; Shen et al., 2022) models. Regarding the data distribution, some models require access to interventions (Brouillard et al., 2020; Ke et al., 2020; Lippe et al., 2021); others assume that $\boldsymbol{N}$ is Gaussian (Kalainathan et al., 2018; Lachapelle et al., 2020) or non-Gaussian (Shimizu et al., 2006); or require non-stationarity (Monti et al., 2019), exchangeability (Guo et al., 2022), or discreteness (Ke et al., 2020) of $\boldsymbol{N}$. Variational-inference–based formulations require a prior over the DAGs (Lorch et al., 2021; 2022; Charpentier et al., 2022) or utilize labels (Yang et al., 2021). Our work was inspired by (Monti et al., 2019), which provides a bivariate CD method for general nonlinear functions and non-stationary data. The authors leverage recent results in NLICA (cf. next section for details) to identify the causal direction. Although they demonstrate applicability to multivariable problems, the use of pairwise independence tests constrains scalability. In our work, we extend these results with an end-to-end solution in § 3.

Identifiability and ICA. Independent Component Analysis (ICA) (Comon, 1994; Hyvärinen et al., 2001) models the observed variables $\boldsymbol{X}$ as a mixture of *independent* variables $\boldsymbol{N}$ via a deterministic function $\boldsymbol{f}$, and focuses on defining models that are *identifiable*—i.e., $\boldsymbol{N}$ can be recovered up to indeterminacies (e.g., scaling, permutation, sign flips, element-wise transformations). Since this is provably impossible in the nonlinear case without further assumptions (Darmois, 1951; Hyvärinen & Pajunen, 1999; Locatello et al., 2019), recent work has focused on incorporating *auxiliary* variables (Hyvärinen et al., 2019; Gresele et al., 2019; Khemakhem et al., 2020a; Gassiat et al., 2022), exploiting temporal structure in the data (Hyvärinen & Morioka, 2017; 2016; Hälvä & Hyvärinen, 2020; Morioka et al., 2021; Monti et al., 2019; Hyvärinen et al., 2010; Klindt et al., 2021; Zimmermann et al., 2021), or restricting the model class (Shimizu et al., 2006; Hoyer et al., 2008; Zhang & Hyvärinen, 2009; Gresele et al., 2021). Several works have related (nonlinear) ICA to SEM estimation (Gresele et al., 2021; Monti et al., 2019; Shimizu et al., 2006; Von Kügelgen et al., 2021; Hyvärinen et al., 2023) by inverting the DGP—i.e., estimating $\boldsymbol{f}^{-1}$ with an *inference model* $\widehat{\boldsymbol{f}}^{-1}$.

3 Inferring causal structure from Jacobians

3.1 Intuition

The method we propose can be intuitively understood as a nonlinear extension of LiNGAM (Shimizu et al., 2006; Hoyer et al., 2008; Peters et al., 2011). LiNGAM assumes a linear causal relationship between observations $\boldsymbol{X}$ and the noise variables $\boldsymbol{N}$, i.e., $\boldsymbol{X} = \mathbf{W}\boldsymbol{N}$. Since the noise variables are assumed to be statistically independent, linear ICA can uncover the (non-Gaussian) sources $\boldsymbol{N}$ from the observations $\boldsymbol{X}$, which allows us to extract the DAG from $\mathbf{W}^{-1}$ as we show in the following example.

Example 1 (Motivating example for linear SEMs)**.** *Assume a linear causal model with three variables, the DAG $X_1 \to X_2 \to X_3$, and functional relationships: $X_1 := N_1$; $X_2 := aX_1 + N_2$; $X_3 := bX_2 + N_3 : a, b \in \mathbb{R}\setminus\{0\}$. The DGP generates samples according to the DAG and has the matrix form on the left—we focus on the elements below the main diagonal as for recovering the DAG, only the paths (i.e., series of directed edges) between X_i and X_j are required and the main diagonal expresses the $N_i \to X_i$ edges. Inverting the DGP with an inference model (i.e., expressing N_i as a function of X_j; LiNGAM uses ICA to estimate the DGP) yields the matrix on the right with elements below the main diagonal capturing the DAG's $X_i \to X_j$ edges (as shown by color coding):*

$$\begin{bmatrix} X_1 \\ X_2 \\ X_3 \end{bmatrix} = \begin{bmatrix} 1 & 0 & 0 \\ a & 1 & 0 \\ ab & b & 1 \end{bmatrix} \begin{bmatrix} N_1 \\ N_2 \\ N_3 \end{bmatrix}; \qquad \begin{bmatrix} N_1 \\ N_2 \\ N_3 \end{bmatrix} = \begin{bmatrix} 1 & 0 & 0 \\ -a & 1 & 0 \\ 0 & -b & 1 \end{bmatrix} \begin{bmatrix} X_1 \\ X_2 \\ X_3 \end{bmatrix}$$

Overview of theoretical results. Our method extends LiNGAM to nonlinear DGPs. First, we show that the inverse DGP's Jacobian and the DAG structure are structurally equivalent (Prop. 1). To apply Prop. 1 to a learned inference model, we describe up to what indeterminacies the inference model is need to be known. Because the ground-truth DGP can only be identified up to certain indeterminacies like scaling, permutation, and sign flips, we need to show for which identifiability notion structural equivalence is preserved (Prop. 2). This requires that we can resolve permutation indeterminacies, which we prove for SEMs in Lem. 1, then design an algorithm for this purpose (§ 3.4).

3.2 DAG equivalence

To justify using the Jacobian of $\boldsymbol{f}^{-1}$, i.e., the inverse of the DGP, (denoted as $\mathbf{J}_{\boldsymbol{f}^{-1}}$), akin to LiNGAM's use of a weight matrix, we first connect the DAG and $\mathbf{J}_{\boldsymbol{f}^{-1}}$ via fundamental concepts from graph theory. The *adjacency matrix* $\boldsymbol{\mathcal{A}}$ of a graph with d nodes is a binary $d \times d$ matrix where each matrix element indicates the presence, or absence, of an edge (i.e., a direct connection) between a pair of nodes X_i, X_j (Defn. A.8). The *connectivity matrix* $\boldsymbol{\mathcal{C}}$ of a graph with d nodes is a binary $d \times d$ matrix where each matrix element indicates the presence, or absence, of a *directed path* between two nodes X_i, X_j (Defn. A.9). For DAGs, both $\boldsymbol{\mathcal{A}}$ and $\boldsymbol{\mathcal{C}}$ are *strictly lower-triangular*—this is why we considered only the elements below the main diagonal in Ex. 1. Furthermore, the main diagonal of $\mathbf{J}_{\boldsymbol{f}^{-1}}$ has non-zero elements (Ex. 1). We describe the relationship between $\mathbf{J}_{\boldsymbol{f}^{-1}}$ and $(\mathbf{I}_d - \boldsymbol{\mathcal{A}})$ for a DAG via *structural equivalence*, and investigate its symmetries. Ex. 1 intuits why our claim refers to $\boldsymbol{\mathcal{A}}$ and not $\boldsymbol{\mathcal{C}}$: in the matrix mapping from $\boldsymbol{X}$ to $\boldsymbol{N}$ only the edges (captured by $\boldsymbol{\mathcal{A}}$) are present. Similar to the linear case (and shown more formally below), $\mathbf{J}_{\boldsymbol{f}^{-1}}$ and $(\mathbf{I}_d - \boldsymbol{\mathcal{A}})$ have the same sparsity structure, meaning $\forall i, j\ (\mathbf{J}_{\boldsymbol{f}^{-1}})_{ij} = 0 \Leftrightarrow (\mathbf{I}_d - \boldsymbol{\mathcal{A}})_{ij} = 0$. We denote this structural equivalence as $\mathbf{J}_{\boldsymbol{f}^{-1}} \sim_{DAG} (\mathbf{I}_d - \boldsymbol{\mathcal{A}})$, with the full definition and its properties formalized as:

Definition 1 ($\sim_{DAG}$)**.** *Two matrices $\mathbf{S}, \mathbf{R}$ of same dimensions are structurally equivalent if $(\mathbf{S})_{ij} = 0 \iff (\mathbf{R})_{ij} = 0 : \forall i, j;$. Structural equivalence, denoted as $\sim_{DAG}$, has the following properties ($\circ$ denotes composition):*

(i) ***$\mathbf{D}$-invariance:*** *a non-singular diagonal matrix $\mathbf{D}$ preserves the sparsity structure; thus, $(\mathbf{D} \circ \mathbf{S}) \sim_{DAG} \mathbf{S}$*

(ii) ***h_0-invariance:*** *for zero-preserving transformations $h_0 : (h_0(\mathbf{S}))_{ij} = 0 \iff (\mathbf{S})_{ij} = 0$ then $h(\mathbf{S}) \sim_{DAG} \mathbf{S}$*

(iii) ***π-equivariance:*** *a permutation π affects the positions of zeros; thus, both operands need to be permuted with the same π to maintain $\sim_{DAG}$, i.e., $\mathbf{S} \sim_{DAG} \mathbf{R} \iff (\pi \circ \mathbf{S}) \sim_{DAG} (\pi \circ \mathbf{R})$,*

(iv) ***Transitivity:*** $\mathbf{S} \sim_{DAG} \mathbf{P} \wedge \mathbf{P} \sim_{DAG} \mathbf{R} \implies \mathbf{S} \sim_{DAG} \mathbf{R}$

(v) ***Commutativity:*** $\mathbf{S} \sim_{DAG} \mathbf{R} \iff \mathbf{R} \sim_{DAG} \mathbf{S}$.

Before proving structural equivalence, we state our assumptions about the SEM:

Assumption 1 (SEM assumptions)**.** *We assume that the causal DGP fulfils:*

(i) The SEM generative model is given by (1)*, for which there exists an underlying DAG;*

(ii) N_i *are jointly independent;*
(iii) There are no hidden confounders (faithfulness/stability); moreover, the Jacobians $\mathbf{J}_{\boldsymbol{f}}$, $\mathbf{J}_{\boldsymbol{f}^{-1}}$ *are structurally faithful (Assum. A.1);*
(iv) each f_i *is bijective; and*
(v) each X_i *depend on* N_i *(i.e.,* $\frac{\partial \boldsymbol{f}(\boldsymbol{X},\boldsymbol{N})}{\partial \boldsymbol{N}}\big|_{\boldsymbol{X},\boldsymbol{N}}$ *is diagonal with non-zero elements)*

Relying on the properties of $\sim_{DAG}$, we prove that $\mathbf{J}_{\boldsymbol{f}^{-1}}$ can be used to extract the DAG for nonlinear SEMs under Assum. 1 (akin to the linear case shown in Ex. 1; the proof is deferred to Appx. E.2)

Proposition 1. *[*$\mathbf{J}_{\boldsymbol{f}^{-1}} \sim_{DAG} (\mathbf{I}_d - \boldsymbol{\mathcal{A}})$*]The inverse DGP's Jacobian* $\mathbf{J}_{\boldsymbol{f}^{-1}}$ *is structurally equivalent to* $(\mathbf{I}_d - \boldsymbol{\mathcal{A}})$*, when Assum. 1 holds.*

Proof (Sketch). From the iterative formulation of the SEM in eq. (2), we note that $\boldsymbol{X}$ (or more precisely, $\boldsymbol{X}(\boldsymbol{N})$), is a fixpoint of $\boldsymbol{f}$. Thus, when we apply the chain rule to calculate $\mathbf{J}_{\boldsymbol{f}}$, we will only have two types of terms (on both sides), namely:

$$\mathbf{A} := \frac{\partial \boldsymbol{f}(\boldsymbol{X},\boldsymbol{N})}{\partial \boldsymbol{X}}\Big|_{\boldsymbol{X},\boldsymbol{N}};\ \mathbf{B} := \frac{\partial \boldsymbol{f}(\boldsymbol{X},\boldsymbol{N})}{\partial \boldsymbol{N}}\Big|_{\boldsymbol{X},\boldsymbol{N}}. \tag{3}$$

This expression leads us to a closed form of $\mathbf{J}_{\boldsymbol{f}}$. Then we apply the inverse function theorem at $(\boldsymbol{X}, \boldsymbol{N})$ to get $\mathbf{J}_{\boldsymbol{f}^{-1}}$. As the last step, we incorporate the indeterminacies—coming from strong identifiability—and show based on the properties of $\sim_{DAG}$ that the statement of the proposition holds. □

Prop. 1 implies that we can extract the DAG from $\boldsymbol{f}^{-1}$; i.e., we can reason about interventions (cf. § 2). We note that if $\mathbf{B} = \mathbf{I}_d$, then (29) describes Additive Noise Models (ANMs) (Hoyer et al., 2008), whereas when additionally $\mathbf{A}$ is constant, we recover LiNGAM (Shimizu et al., 2006). Prop. 1 assumes that we have access to $\boldsymbol{f}^{-1}$; however, this is a non-trivial assumption. In the following, we investigate to what extent we need to estimate $\boldsymbol{f}^{-1}$ (in form of $\widehat{\boldsymbol{f}}^{-1}$) to exploit Prop. 1—for this, we leverage the notion of identifiability.

3.3 Identifiability requirements of $\widehat{\boldsymbol{f}}^{-1}$

The inference model $\widehat{\boldsymbol{f}}^{-1}$ we learn from the observed data generally differs from the true inverse of $\boldsymbol{f}$ up to certain indeterminacies depending on the identifiability guarantees of the (most commonly) NLICA algorithm. This can include scaling, permutation, sign flips, and monotonic element-wise transformations (Hyvärinen et al., 2001; Khemakhem et al., 2020a; Zimmermann et al., 2021). While element-wise transformations such as scaling or sign-flips do not influence the sparsity structure of the Jacobian, permutations break structural equivalence between the Jacobian and the ground-truth adjacency matrix. That is, we need to resolve the permutation indeterminacy to apply Prop. 1 to $\mathbf{J}_{\widehat{\boldsymbol{f}}^{-1}}$. With the right ordering(s)[2], the Jacobian $\mathbf{J}_{\widehat{\boldsymbol{f}}^{-1}}$ features a lower-triangular structure. The following lemma shows that this property determines the ordering of the noise variables such that they yield a lower-triangular Jacobian, i.e., all possible causal orderings that ensure structural equivalence to the ground-truth adjacency matrix (the proof is deferred to Appx. E.1):

Lemma 1. *[DAG DGPs resolve the permutation ambiguity of ICA] When the DGP is a SEM with functional relationships* $\boldsymbol{f}$ *and an underlying DAG, then the permutation indeterminacy of ICA* π_{ICA} *can be accounted for such that the Jacobian of the inference network will have a lower-triangular Jacobian, even with unknown causal ordering* π*.*

Proof (Sketch). Given that the DGP is structured by a DAG, the adjacency matrix $\boldsymbol{\mathcal{A}}$ is lower triangular and Assum. 1 ensures that diagonal elements are nonzero. The permutation indeterminacy of ICA (which is expressed as a left-multiplication, i.e., affects the rows) comprises matrices that do not violate lower-triangularity. This gives us a single permutation (for a unique causal ordering) or a set of permutations, each of which ensures a lower triangular $\boldsymbol{\mathcal{A}}$. □

We emphasize that Lem. 1 refers to *two permutations*: the permutation indeterminacy of ICA (Lem. 1 makes a claim about this) and the causal ordering of the SEM. These can be thought of as permuting the rows (ICA indeterminacy) and columns (causal ordering) of the inference model's Jacobian. Most importantly, Lem. 1 shows that we can resolve the permutation indeterminacy, leading to the following result:

[2]The causal ordering does not need to be unique, e.g., in the DAG $X_i \leftarrow X_j \rightarrow X_k$ the nodes X_i and X_k are interchangeable

Algorithm 1 Algorithm for multivariable CD and determining the causal order π

Input: dataset D, network parameters θ, Sinkhorn networks $\mathbf{S}_{\text{ICA}}, \mathbf{S}_\pi$, contrastive loss $\mathcal{L}_{\text{CL}}$ (eq. (6)), ordering loss $\mathcal{L}_\pi$ (eq. (5)), positive scalars $\alpha_d, \alpha_u, \alpha_l$
Initialize θ
while $\mathcal{L}_{\text{CL}}$ not converged **do**
  calculate $\mathcal{L}_{\text{CL}}$ for a batch from D
  update θ
end while
extract $\mathbf{J}_{\widehat{\boldsymbol{f}}^{-1}}$
while $\mathcal{L}_\pi$ not converged **do**
  $\mathbf{K} = \left|\mathbf{S}_{\text{ICA}} \mathbf{J}_{\widehat{\boldsymbol{f}}^{-1}} \mathbf{S}_\pi\right|$
  $\mathcal{L}_\pi = \sum_{i,j} \left[\alpha_d \left(\mathbf{K}\right)_{ii}^{-1} - \alpha_l \left(\mathbf{K}\right)_{i \geq j} + \alpha_u \left(\mathbf{K}\right)_{i<j}\right]$
  update $\mathbf{S}_{\text{ICA}}, \mathbf{S}_\pi$
end while

Proposition 2 ($\mathbf{J}_{\boldsymbol{f}^{-1}} \sim_{DAG} \mathbf{J}_{\widehat{\boldsymbol{f}}^{-1}}$ for strongly identified $\widehat{\boldsymbol{f}}^{-1}$)**.** *When the inference model $\widehat{\boldsymbol{f}}^{-1}$ is strongly identified in the sense of Defn. B.1, the permutation indeterminacies are resolved, and Assum. 1 holds, then $\mathbf{J}_{\boldsymbol{f}^{-1}} \sim_{DAG} \mathbf{J}_{\widehat{\boldsymbol{f}}^{-1}}$.*

Proof. The indeterminacies of strong identifiability (Defn. B.1) include scalings, sign flips, and permutations. By Def. 1(i), $\sim_{DAG}$ is invariant to scalings and sign flips; whereas Def. 1(iii) states equivariance for permutations, but by Lem. 1, those can be resolved for SEMs. □

By Def. 1(ii), Prop. 2 also holds when indeterminacies include zero-preserving transformations.

3.4 Algorithm for CD and determining π

Based on Lem. 1 and Props. 1 and 2, we propose a two-step approach for extracting the DAG from observational but non–i.i.d. data for general nonlinear $\boldsymbol{f}$:

1. First, we use a suitable nonlinear ICA algorithm to estimate $\boldsymbol{f}^{-1}$ up to permutations and zero-preserving element-wise nonlinearities with an inference model $\mathbf{J}_{\widehat{\boldsymbol{f}}^{-1}}$.
2. Second, we resolve the permutation indeterminacy by accounting for the causal graph structure.

Regarding the second step, we learn the permutations after training with an objective that enforces the estimated Jacobian to be lower-triangular. To this end, we need to learn both a permutation π for the causal ordering as well as a permutation π_{ICA} that resolves the indeterminacy in the noise variables introduced by ICA. We use the permuted absolute Jacobian $\mathbf{K}$ defined as

$$\mathbf{K} := \left|\mathbf{S}_{\text{ICA}} \mathbf{J}_{\widehat{\boldsymbol{f}}^{-1}} \mathbf{S}_\pi\right| \tag{4}$$

where $\mathbf{S}_{\text{ICA}}, \mathbf{S}_\pi$ are doubly-stochastic matrices that represent a soft permutation on both noise and observation variables, which we parametrize via Sinkhorn networks (Mena et al., 2018) and learn after ICA training—cf. § 5.1 and Fig. 10 for details. We then introduce a training loss inspired by LiNGAM (Shimizu et al., 2006) that encourages $\mathbf{K}$ to be lower-triangular by simultaneously maximizing i) the sum of the main diagonal and ii) the lower-triangular part, while also iii) minimizing the stricly-upper triangular part of $\mathbf{K}$,

$$\mathcal{L}_\pi = \sum_{i,j} \left[\alpha_d \left(\mathbf{K}\right)_{ii}^{-1} - \alpha_l \left(\mathbf{K}\right)_{i \geq j} + \alpha_u \left(\mathbf{K}\right)_{i<j}\right], \tag{5}$$

where $i \in \{d, u, l\} : \alpha_i > 0$ The full learning algorithm is presented in Alg. 1.
Compared to LiNGAM, our method is differentiable and works for nonlinear SEMs; thus, it does not require iterating over all permutations. Although Sinkhorn networks (Mena et al., 2018) were previously proposed to represent permutation probabilities (Charpentier et al., 2022), we are the first to represent the indeterminacy of ICA with such models.

4 Identifiability in Contrastive Learning

There are fundamental limits to how much one can learn about a DGP from only i.i.d. observations: neither causal structure (Pearl, 2009), nor nonlinear mixing of independent signals (Hyvärinen & Pajunen, 1999) are identifiable in the general case. In this work, we describe a non–i.i.d. (contrastive) DGP, in which significantly more structure can be identified from observations.

In a contrastive DGP (Zimmermann et al. (2021); § 4.2), we generate so-called positive pairs containing two d–dimensional samples $(\boldsymbol{X}, \widetilde{\boldsymbol{X}})$. Underlying $\boldsymbol{X}$ and $\widetilde{\boldsymbol{X}}$ are a pair of latent variables of the same dimension $\boldsymbol{N}$ and $\widetilde{\boldsymbol{N}}$, such that $\boldsymbol{X} = \boldsymbol{f}(\boldsymbol{N})$ and $\widetilde{\boldsymbol{X}} = \boldsymbol{f}(\widetilde{\boldsymbol{N}})$. Both $\boldsymbol{N}$ and $\widetilde{\boldsymbol{N}}$ have statistically independent components, i.e. $\forall i, j : N_i \perp N_j$ and $\widetilde{N}_i \perp \widetilde{N}_j$. Furthermore, each component of $\widetilde{\boldsymbol{N}}$ depends only on the corresponding component of $\boldsymbol{N}$, such that $\forall i : \widetilde{N}_i \sim p(\cdot|N_i)$. In this work, we will often assume that the mapping $\boldsymbol{f}$ is defined as a SEM (§ 2).

4.1 Identifiability of causal graphs via the ICM principle

In the contrastive DGP, we draw i.i.d. samples of positive pairs. Inasmuch as we consider $\boldsymbol{X}$ and $\widetilde{\boldsymbol{X}}$ as two observations, the generative process is non–i.i.d.. This non–i.i.d. DGP leaves more fingerprints in the observed data, allowing the identification of causal dependencies that are non-identifiable in the i.i.d. case. We will illustrate why this is the case in the following two-variable example.

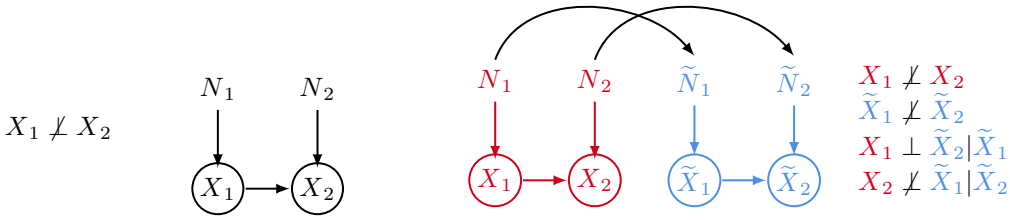

(a) No data augmentation.

(b) Data augmentation. Superscripts denote the two components of the positive pair.

Figure 2: Comparing conditional independencies between observables $\widetilde{X}_i$ in a bivariate model without (Fig. 2a) and with (Fig. 2b) data augmentations in the contrastive pair.

Example 2 (Positive pairs induce additional conditional independencies)**.** *Assume a bivariate, faithful SEM without confounders, where $X_1 \to X_2$ (Fig. 2a). Observing only i.i.d. copies of X_1 and X_2, the direction of the cause–effect relationship cannot be discerned, the only statement we can make is $X_1 \not\perp X_2$ (Pearl, 2009). However, consider observing positive pairs from the contrastive DGP, illustrated graphically in (Fig. 2b). As $\boldsymbol{X}$ and $\widetilde{\boldsymbol{X}}$ are dependent, there is a broader set of conditional independence statements we can make, and these resolve the ambiguity in the causal direction. Namely, X_1 (the cause component of $\boldsymbol{X}$) and $\widetilde{X}_2$ (the effect component of $\widetilde{\boldsymbol{X}}$) are statistically dependent via the path $X_1 \leftarrow N_1 \to \widetilde{N}_1 \to \widetilde{X}_1 \to \widetilde{X}_2$. However, conditioning on $\widetilde{X}_1$ blocks this path, thus $X_1 \perp \widetilde{X}_2 | \widetilde{X}_1$. Notably, such a conditional independence holds only when $X_1 \to X_2$, but would not hold, if the direction were reversed to $X_1 \leftarrow X_2$.*

Ex. 2 sheds light how Contrastive Learning (CL) enables CD by introducing additional conditional independencies in the positive pair. This line of reasoning connects our work to the Causal de Finetti (CdF) theorem (Guo et al., 2022), which proves identifiability of fully observed causal graphs under a very similar generative process. The key concept in the CdF is the notion of Independent Causal Mechanisms (ICM). That is, the assumption that various mechanisms that make up the generative process (e.g., individual equations in a SEM) change or vary in a statistically independent manner. In our generative model, when $\boldsymbol{f}$ is a SEM, the ICM principle manifests in the assumption that $\forall i \neq j : N_i \perp \widetilde{N}_j$. One can thus think of $\widetilde{\boldsymbol{X}}$ as an observed counterfactual outcome, where the structural equations have been independently perturbed.

Exploiting the connection to CdF, one can show that in our generative process, all causal relationships become identifiable even in multivariable data in the absence of unobserved (confounder) variables. While showing this is somewhat involved in the asymmetric contrastive DGP of Zimmermann et al. (2021) presented

here, other variants of contrastive DGPs—including the original model proposed in SimCLR (Chen et al., 2020) or (Dubois et al., 2022)—produce exchangeable positive pairs by relying on two augmented samples $(\widetilde{\boldsymbol{X}}^1, \widetilde{\boldsymbol{X}}^2)$, and thus map directly to the CdF setting.
Showing that causal relationships are identifiable from the conditional independence structure in CL is mathematically interesting, but does not yield a practical algorithm. As noted by Guo et al. (2022), the CdF requires an exponential number of conditional independence tests for multivariable CD. Here, we take a different approach, that exploits the full identifiability of the functional relationships $\boldsymbol{f}$ in the same setting.

4.2 Identifiability of the causal graph via identifiability of $\boldsymbol{f}$

We assume the setting of (Zimmermann et al., 2021, Thm. 6)—with the additional constraint that $\dim \boldsymbol{N} = \dim \boldsymbol{X} = d$—, under which, an inference model $\widehat{\boldsymbol{f}}^{-1}$ which minimizes a contrastive loss was proven to estimate the noise variables (often referred to as "sources" in the ICA literature) up to a composition of input independent permutations, sign flips, and rescaling. For completeness, we restate the assumptions both for the DGP (Assum. 2) in the main text and defer the model assumptions (Assum. F.1) to the appendix (Appx. F). We denote positive pairs with $\widetilde{(\cdot)}$ and negative pairs with $(\cdot)^-$.

Assumption 2 (DGP on $\mathbb{R}^d$)**.** *We assume that the DGP satisfies the following conditions:*

(i) The space of the noise variables to be a convex body (hyperrectangle); i.e., $\mathcal{N} \subseteq \mathbb{R}^d$;
(ii) The observation space to be $\mathcal{X} \subseteq \mathbb{R}^d$;
(iii) The generator (the SEM) $\boldsymbol{f}$ to
  1. be bijective,
  2. map $\mathcal{N} \subseteq \mathbb{R}^d \to \mathcal{X}$, and
  3. be differentiable in the vicinity of $\mathcal{N}$.
(iv) The marginal distribution $p(\boldsymbol{N})$ over latent variables $\boldsymbol{N} \in \mathcal{N}$ is uniform[3]; i.e., $p(\boldsymbol{N}) = |\mathcal{N}|^{-1}$;
(v) The conditional distribution over positive pairs $p(\widetilde{\boldsymbol{N}}|\boldsymbol{N})$ is a rotationally asymmetric generalized normal distribution (Subbotin, 1923) with a shape parameter of one (Laplace distribution)[4]; i.e., $p(\widetilde{\boldsymbol{N}}|\boldsymbol{N}) = C_p^{-1}(\boldsymbol{N}) e^{-\lambda \left|\boldsymbol{N} - \widetilde{\boldsymbol{N}}\right|}$ with $C_p := \int e^{-\lambda \left|\boldsymbol{N} - \widetilde{\boldsymbol{N}}\right|} d\widetilde{\boldsymbol{N}}$, where $\lambda > 0$ a parameter controlling the width of the distribution and δ is the L_1 metric.

We parametrize the conditional distribution $q(\widetilde{\boldsymbol{N}}|\boldsymbol{N})$ via $\boldsymbol{f}^{-1}$ as in Assum. 2 and calculate the loss as:

$$\mathbb{E}_{(\boldsymbol{X}, \widetilde{\boldsymbol{X}}, \boldsymbol{X}^-)} \left[-\log \frac{\exp\left[-\left| \widehat{\boldsymbol{f}}^{-1}(\boldsymbol{X}) - \widehat{\boldsymbol{f}}^{-1}(\widetilde{\boldsymbol{X}}) \right| / \boldsymbol{\tau} \right]}{\exp\left[-\left| \widehat{\boldsymbol{f}}^{-1}(\boldsymbol{X}) - \widehat{\boldsymbol{f}}^{-1}(\widetilde{\boldsymbol{X}}) \right| / \boldsymbol{\tau} \right] + \sum_i^M \exp\left[-\left| \widehat{\boldsymbol{f}}^{-1}(\boldsymbol{X}^-) - \widehat{\boldsymbol{f}}^{-1}(\widetilde{\boldsymbol{X}}) \right| / \boldsymbol{\tau} \right]} \right], \tag{6}$$

where $\widetilde{\boldsymbol{X}}$ is the positive pair, $\boldsymbol{X}^-$ are the negative pairs, and M is the number of negative samples. During training one has access to observations $\boldsymbol{X}$, which are samples from these distributions transformed by the generator function (i.e., the SEM) $\boldsymbol{f}$.

Differences between identifying the DAG and $\boldsymbol{f}$. Assum. 2 implies restrictions on the class of SEM we can represent in this framework. In particular, Assum. 2(iv) requires that the noise variables are uniform. This however, is a minimal restriction, considering that any real-valued random variable can be emulated by passing a uniform random variable through its inverse cumulative distribution function (CDF). Thus, so long as the inverse CDF is differentiable, we can absorb it into $\boldsymbol{f}$ without modifying the causal structure implied by the SEM. Assum. 2(v) relates to the type of random perturbation under which the positive pairs are generated. We note that Assum. 2 is specific to the contrastive ICA framework of (Zimmermann et al., 2021) but our approach is not fundamentally limited to the this setting, and can be used in principle in any situation where nonlinear ICA is identifiable, such as in (Hyvärinen & Morioka, 2016; 2017; Morioka et al., 2021; Monti et al., 2019).
That is, our results state that identifiability of $\boldsymbol{f}$ entails identifiability of the causal graph. However, this is not necessarily true in the other direction, since knowing the Jacobian (which is sufficient to recover the

[3]Since any random variable in $\mathbb{R}^d$ can be emulated by passing a uniformly distributed random variable through the corresponding inverse CDF, if the CDF is differentiable, we can abosrb it into $\boldsymbol{f}$

[4]We fix the shape parameter to one, since we use the Laplace distribution in our experiments, but identifiability holds for all shapes α with the corresponding L_α-metric, where $\alpha \geq 1 \wedge \alpha \neq 2$. We note that certain transitions in natural videos seem to follow the Laplace distribution (Klindt et al., 2021), justifying this choice

DAG) does not contain all information about $\boldsymbol{f}$. It remains an open question how practically relevant these differences are.

5 Experiments

5.1 Experimental setup

Data Generating Process (DGP). We experiment with three DGPs: i) linear and ii) nonlinear SEMs (in the form of $\boldsymbol{X} = \boldsymbol{f}(\mathbf{W}\boldsymbol{N})$, as well as with iii) Multi-Layer Perceptrons (MLPs) with triangular weight matrices (as used in (Monti et al., 2019)). In all cases, the nonlinear activations (i.e., $\boldsymbol{f}$) are leaky ReLUs (with a slope of 0.25 for the SEMs and 0.1 for the triangular MLPs). For the SEM DGPs, we exlore three options: a) no permutation w.r.t. the causal ordering (i.e., only the ICA permutation remains); b) a sparse DGP (with each $X_i - X_j$ edge being nonzero with a 0.25 probability); and c) permuted causal ordering (with dense $\boldsymbol{\mathcal{A}}$). Additionally, we ensure that the ordering of N_i is unique (all cases), and that the DGP weights are $\gg 0$ (for the SEM DGPs) as otherwise we would be unable to distinguish weak connections from small elements in the Jacobian. That is, the estimate of a weak connection could be the same order of magnitude as the estimate of a zero element due to the stochasticity of training—we do not enforce this property for the triangular MLPs to compare to the results of (Monti et al., 2019), where such modification was not present. For the *permuted* SEM DGPs, we sample 6 different orderings and 5 seeds for each problem dimensionality $\{3; 5; 8; 10\}$—the number of seeds is 10 for non-permuted and sparse SEMs. For the triangular MLP, we use $d = 6$ and 5 seeds to compare to (Monti et al., 2019, Fig. 2) and vary the number of layers in the mixing. To use contrastive NLICA for training the inference model, the DGPs needs to satisfy the assumptions underlying the proof of identifiability (Zimmermann et al., 2021, Thm. 6)): the latent space is a hyperrectangle in $\mathbb{R}^d$, the marginal $p(\boldsymbol{N})$ is uniform, the conditional $p(\widetilde{\boldsymbol{N}}|\boldsymbol{N})$ is Laplace, $\boldsymbol{X}$ is generated by a smooth and bijective mapping;

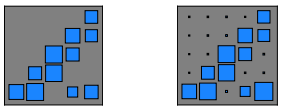

Figure 3: Hinton diagrams ($d = 5$): ground truth (left), estimate (right). Size equals magnitude.

Inference model. To (strongly) identify the SEM, we use contrastive NLICA (Zimmermann et al., 2021)—which is consistent when the number of negative samples goes to infinity—to estimate $\widehat{\boldsymbol{f}}^{-1}$ with a hyperrectangle latent space in $\mathbb{R}^d$ and the contrastive loss uses the same metric as the conditional, which is L_1 for our case (Assums. 2 and F.1). Our architecture for the inference model is the same MLP as in (Zimmermann et al., 2021) (Tab. 6). To account for the permutation indeterminacies, we use two Sinkhorn networks (Mena et al., 2018) (similar to Charpentier et al. (2022)). A Sinkhorn network is a trainable parametrization of soft-permutation matrices (the Birkhoff polytope) (Mena et al., 2018), consisting of two levels: i) the Sinkhorn operator (Fig. 10) normalizes each row and column (in this order) of a matrix to one, relyin on the log-sum-exp operator; ii) the network layer contains the trainable matrix $\mathbf{W}$ with the scalar temperature value $\boldsymbol{\tau}$ to ensure convergence to the Birkhoff polytope's vertices, i.e., to yield a (hard) permutation matrix. We observed that setting the lowest $d\,(d-1)\,/2$ elements (for dense DAGs) to zero and converting the resulting $\mathbf{K}$ matrix to binary often helped the convergence of the Sinkhorn networks. We calculate the Jacobian of the inference model with the `autograd` module of PyTorch (Paszke et al., 2019) in the forward pass and vectorize the operation with the recently released `functorch` library (Horace He, 2021). Moreover, instead using max to aggregate the different Jacobians over the batch, we found using the mean operator more stable in practice.

Metrics. We measure learning the correct ordering by the ordering accuracy (Acc_π, only for the permuted case)—i.e., the ratio of causal variable pairs $\forall i < j : (N_i, N_j)$, such that the ranking (expressed by $\text{sign}\,(i-j)$) matches that in the inferred (permuted) ordering π, i.e., $\text{sign}\,(\pi\,(i) - \pi\,(j))$. To normalize, we divide by the number of distinct edge pairs ($1/2(d-1)d$) We also report the accuracy (Acc, i.e., the ratio of correctly identified edges, or lack thereof, divided by $|\mathcal{E}^*|$) and the Structural Hamming Distance (SHD) (we use 1e−3 as the threshold in all scenarios) for inferring the edges of the DAG, as is standard practice in the literature (Lachapelle et al., 2020; Monti et al., 2019; Ke et al., 2020; Vowels et al., 2022).

Comparison. We use the linear and nonlinear SEM DGPs to showcase that our method can infer the DAG while also learning the correct ordering. Then, we compare to NonSENS (Monti et al., 2019), which,

Table 1: Validation of Lem. 1 for linear and nonlinear SEMs with **unknown causal ordering** to measure how well our method recovers the causal ordering. Mean Correlation Coefficient (MCC) measures identifiability, $|\mathcal{E}^*|$ is the maximum number of edges in a DAG, Acc_π is the accuracy of recovering the pairwise causal ordering π, whereas π gives the ratio of learning a (any) permutation in $\mathbf{S}_\pi$ and SHD is the Structural Hamming Distance

		Linear					Nonlinear				
$\lvert\mathcal{E}^*\rvert$	d	MCC	Acc	Acc_π	π	SHD	MCC	Acc	Acc_π	π	SHD
6	3	1.	1.	1.	1.	0.	1.	1.	1.	1.	0.
15	5	$0.989_{\pm 0.039}$	$0.998_{\pm 0.009}$	$0.974_{\pm 0.078}$	0.76	$0.002_{\pm 0.009}$	$0.988_{\pm 0.039}$	$0.994_{\pm 0.021}$	$0.957_{\pm 0.129}$	0.583	$0.006_{\pm 0.021}$
36	8	$0.834_{\pm 0.238}$	$0.935_{\pm 0.081}$	$0.851_{\pm 0.183}$	0.414	$0.065_{\pm 0.081}$	$0.781_{\pm 0.219}$	$0.934_{\pm 0.051}$	$0.889_{\pm 0.15}$	0.345	$0.066_{\pm 0.051}$
55	10	$0.852_{\pm 0.251}$	$0.931_{\pm 0.051}$	$0.921_{\pm 0.147}$	0.233	$0.069_{\pm 0.051}$	$0.794_{\pm 0.255}$	$0.924_{\pm 0.073}$	$0.739_{\pm 0.252}$	0.276	$0.076_{\pm 0.073}$

Table 2: Causal discovery performance for linear and nonlinear SEMs with **known causal ordering**. Mean Correlation Coefficient (MCC) measures identifiability, $|\mathcal{E}^*|$ is the maximum number of edges in a DAG, Acc is accuracy, Ours is our proposal, HSIC refers to using HSIC independence tests, and SHD is the Structural Hamming Distance

		Linear				Nonlinear			
$\lvert\mathcal{E}^*\rvert$	d	MCC	Acc(Ours)	Acc(HSIC)	SHD	MCC	Acc(Ours)	Acc(HSIC)	SHD
6	3	1.	1.	$0.7_{\pm 0.1}$	0.	1.	1.	$0.741_{\pm 0.105}$	$0.049_{\pm 0.14}$
15	5	$0.969_{\pm 0.066}$	$0.928_{\pm 0.131}$	$0.828_{\pm 0.116}$	$0.072_{\pm 0.131}$	$0.94_{\pm 0.09}$	$0.858_{\pm 0.172}$	$0.8_{\pm 0.102}$	$0.142_{\pm 0.171}$
36	8	1.	1.	$0.682_{\pm 0.17}$	0.	$0.982_{\pm 0.029}$	$0.872_{\pm 0.198}$	$0.823_{\pm 0.142}$	$0.128_{\pm 0.198}$
55	10	$0.965_{\pm 0.03}$	$0.832_{\pm 0.176}$	$0.551_{\pm 0.003}$	$0.168_{\pm 0.176}$	$0.962_{\pm 0.025}$	$0.636_{\pm 0.239}$	$0.638_{\pm 0.134}$	$0.364_{\pm 0.239}$

unlike our proposal, does CD on an edge-by-edge basis. Thus, the causal ordering π does not affect how NonSENS operates. We use the HSIC independence test (Gretton et al., 2005) on top of contrastive NLICA (Zimmermann et al., 2021) to provide a close comparison with NonSENS (Monti et al., 2019). Notably, since our assumptions provide identifiability up to generalized permutations, there is no need to perform linear ICA on top of contrastive NLICA. Thus, we test independence between the observations X_i and the *inferred* noise variables $\hat{N}_j$—although the number of tests is d^2, we use a Bonferroni correction factor of 4, since each edge is determined based on four tests (Monti et al., 2019).

5.2 Results

In all experiments except those in Tab. 1, we used the output of the matching problem as an oracle (solved via the Hungarian algorithm (Kuhn, 1955)) to correct for the permutation indeterminacy of ICA.

The permutation indeterminacies can be resolved (verifying Lem. 1). Tab. 1 corroborates the result of Lem. 1: it is possible to resolve the permutation indeterminacy by assuming a DAG DGP. However, Acc_π strongly depends on the performance of NLICA, measured by Mean Correlation Coefficient (MCC). As MCC deteriorates, the correct causal ordering cannot be recovered. Nonetheless, erroneous solutions resulting from training stochasticity (the most frequent problem according to our observations) can be simply filtered out: in this case the doubly stochastic matrices usually do not converge to a permutation matrix. Inspecting their elements or automatically rejecting such solutions is straightforward. Thus, we report two quantities in Tab. 1: Acc_π is the ratio of inferring the order of causal variable pairs *when the Sinkhorn networks converged to permutation matrices*; π (with a slight abuse of notation), on the other hand, reports the ratio of the successful attempts to recover permutation matrices. Clearly, failing to converge to a permutation matrix is the bottleneck of this step, since despite failing to scalably recover π, in case of converging to a permutation matrix the captured graph reflects most of the edges. This is reported by the Acc_π column that is calculated after applying the learned (not necessarily correct) permutations.

Competitive performance on linear and nonlinear SEMs. Tab. 2 demonstrates (with π being known) that our method outperforms HSIC in the linear case and is at least comparable to HSIC in the nonlinear case—note that the entries in $\mathbf{J}_{\widehat{\boldsymbol{f}}^{-1}}$ were ordered by absolute value and the smallest ones were zeroed out—namely, these are the elements of the Jacobian that most probably correspond to the zeros in the true Jacobian. However, this modification might require additional knowledge about the sparsity of the DAG. Fig. 4 describes how precision and recall changes for threshold values from $[1\text{e}{-7}; 1\text{e}0]$ for *sparse* DAGs. Notably, the nonlinear curves are better than the linear ones. For additional results on sparse SEMs (Tab. 7) and SEMs with unknown causal ordering (Tab. 8, evaluation is done after accounting for the causal ordering), cf. Appx. G. For sparse SEMs, HSIC is slightly better for larger graphs, whereas in the case of unknown causal ordering, our proposal has better accuracy in most cases. To visualize the inferred graph structure, we plot a Hinton diagram of the true and estimated Jacobians in Fig. 3, showing that $\mathbf{J}_{\widehat{\boldsymbol{f}}^{-1}}$ can capture the edges of an underlying *sparse* DAG.

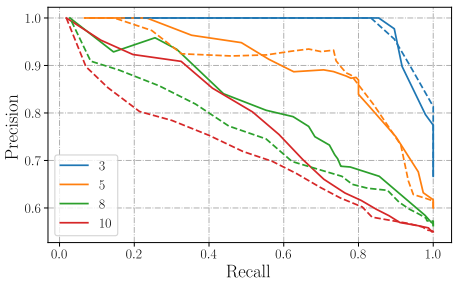

Figure 4: Precision vs recall for thresholds in $[1\text{e}{-7}; 1\text{e}0]$ for linear (dashed) and nonlinear (solid) *sparse* SEMs

Competitive performance on triangular MLPs from (Monti et al., 2019). Tab. 3 summarizes our results with the triangular MLP of (Monti et al., 2019). Despite having small weights in the ground truth Jacobian $\mathbf{J}_{\boldsymbol{f}^{-1}}$ (appr. $2\text{e}{-3}$ for one and $1\text{e}{-8}$ for five layers), our method was able to infer most edges in the DAG. Importantly, the resulting accuracies are larger than those of our adapted version of NonSENS (Monti et al., 2019). Moreover, our method has the advantage of simultaneously inferring all edges based on the structure of $\mathbf{J}_{\widehat{\boldsymbol{f}}^{-1}}$—thus, it does not require d^2 pairwise independence test for a DAG with d nodes. Our application of HSIC independence tests resulted in surprisingly low accuracy, despite utilizing an NLICA method with identifiability guarantees up to generalized permutations. Interestingly, HSIC resulted in (close-to) chance-level performance in our repeated experiments—by careful inspection of the DGP, we found that the weights are in the order of $1\text{e}{-4}$, which might explain such bad performance. As noted above, since Monti et al. (2019) did not constrain the weights, we used a uniform initialization scheme, which might led to mismatching experimental conditions. Though the use of HSIC was inspired by NonSENS (Monti et al., 2019), since we made different assumptions on the DGP, the results only represent HSIC's (but not NonSENS's) performance.

Table 3: Causal discovery performance for the triangular MLP from (Monti et al., 2019) with $d = 6$. $|l|$ denotes the number of MLP layers, Acc the accuracy, Ours is our proposal, HSIC refers to using HSIC independence tests. Chance level is (for the dense MLP) $21/36 = 0.583$

$\lvert l\rvert$	MCC	Acc (Ours)	Acc (HSIC)
1	1.	$0.933_{\pm 0.042}$	0.583
2	1.	0.944	0.583
3	$0.997_{\pm 0.003}$	1.	0.583
4	$0.978_{\pm 0.016}$	$0.922_{\pm 0.097}$	$0.6_{\pm 0.033}$
5	$0.603_{\pm 0.062}$	$0.711_{\pm 0.054}$	$0.589_{\pm 0.011}$

6 Related work

We provide a detailed comparison of related CD methods (Tab. 4) and the use of the Jacobian (Tab. 5) in Appx. D.

Independence tests for CD. Traditional CD methods (Pearl, 2009; Spirtes & Zhang, 2016; Spirtes et al., 2000; Peters et al., 2017) rely on statistical (conditional) independence tests to infer the graph structure. Recent works also leverage such tests (Shimizu et al., 2006; Monti et al., 2019; Guo et al., 2022; Karlsson & Krijthe, 2022) to uncover hidden confounders (Karlsson & Krijthe, 2022), for bivariate (Janzing et al., 2009; Monti et al., 2019) or multivariable CD (Guo et al., 2022) for nonlinear SEMs. LiNGAM (Shimizu et al., 2006), which inspired our work, also relies on independence tests to prune edges. Although independence tests provide additional information via significance values, they are not differentiable and can be costly, as d latents require d^2 tests.

Optimization-based CD. Zheng et al. (2018) introduced the continuous optimization-based NOTEARS algorithm for linear SEMs, which has inspired further research (Khemakhem et al., 2021; Lorch et al., 2021; Ng et al., 2022; Schölkopf et al., 2021; Yu et al., 2019; Lachapelle et al., 2020; Kalainathan et al., 2018) to provide differentiable methods for CD in neural networks. Most of the differentiable solutions (Khemakhem et al., 2021; Ng et al., 2022; Schölkopf et al., 2021; Yu et al., 2019) constrain the function class, some of them (Lachapelle et al., 2020; Kalainathan et al., 2018) both the function class and the data distribution.

Using the adjacency matrix $\boldsymbol{\mathcal{A}}$. Our work shows that the adjacency matrix $\boldsymbol{\mathcal{A}}$ and the Jacobian of the inference model $\mathbf{J}_{\widehat{\boldsymbol{f}}^{-1}}$ can both be used to model the edges in a graph. We review both, starting with the adjacency matrix for CD: Zheng et al. (2018) use $\boldsymbol{\mathcal{A}}$ as a regularizer in NOTEARS, Ng et al. (2022) reformulates the SEM with an adjacency matrix for additive models, Schölkopf et al. (2021) models $\boldsymbol{\mathcal{A}}$ with an LSTM in a variational framework. In (Brouillard et al., 2020), $\boldsymbol{\mathcal{A}}$ appears for the interventional case. Lorch et al. (2022) leverage amortized variational inference for CD, where they deploy multi-head attention Vaswani et al. (2017) and use the softmax probabilities as a proxy for the adjacency matrix (i.e., their model represents the probability of edges in the graph). Charpentier et al. (2022) defines a probabilistic model over $\boldsymbol{\mathcal{A}}$ to differentiably sample DAGs, then use variational inference to estimate the causal structure. The proposed method has strong empirical performance, but does not provide theoretical guarantees for CD.

Using the Jacobian. The Jacobian matrix of either the generative ($\mathcal{N} \to \mathcal{X}$) or the inference ($\mathcal{X} \to \mathcal{N}$) models are used throughout the literature, both for identifiability and CD (Tab. 5). LiNGAM Shimizu et al. (2006) uses the Jacobian (i.e., a constant matrix) to infer the DAG in the linear case, whereas Lachapelle et al. (2020) calculates the Jacobian of the inference network to enforce acyclicity, generalizing to nonlinear additive models. Rolland et al. (2022) consider the same model class as Lachapelle et al. (2020), but they rely on the Jacobian of the score function. Leveraging properties of the Jacobian is also present in the identifiability literature: Independent Mechanism Analysis (IMA) relies on the assumption that the generative model's Jacobian has orthogonal columns Gresele et al. (2021)—our work reasons about the inference network's Jacobian, without functional constraints. Although the inspiration comes from the causal principle of independent mechanisms, the claims are about identifiability and not about CD: the IMA function class is locally identifiable, whereas the subclass of conformal maps are identifiable Buchholz et al. (2022). Similar to IMA, Zheng et al. (2022) also utilize the Jacobian of the generative model and prove identifiability for NLICA under a sparsity assumption. Atanackovic et al. (2023) propose a Bayesian approach for CD in dynamical systems, including cyclic graphs, where they associate the graph's edges with the sparsity pattern of the Jacobian of the SEM (in this case an ODE), but the authors do not prove identifiability. That is, although the use of the Jacobian is prevalent in the literature, to the best of our knowledge, we are the first to use the Jacobian of the inference model for causal models without constraining the function class (but using non–i.i.d. data, while providing identifiability guarantees.

CD from interventions. Many algorithms can incorporate interventions (Brouillard et al., 2020; Ke et al., 2020; Lippe et al., 2021; 2022; Lorch et al., 2021). Interestingly, (Ke et al., 2020) provide an extension of (Yu et al., 2019; Zheng et al., 2018) to interventional data, and of the bivariate method of (Bengio et al., 2020) to a multivariable one. It is remarkably similar to our proposal, as both make assumptions only on the data (i.e., admitting general nonlinear functional relationships), but as (Ke et al., 2020) requires interventions, its path is orthogonal to ours. So is the work of (Lippe et al., 2021), which removes any requirement on the data, scales to multiple variables, but requires interventions.

7 Discussion

Limitations. Our theory requires the guarantees of strong identifiability but not the use of a specific (NLICA) algorithm. Though our experiments demonstrate that fulfilling strong identifiability is sufficient for CD, we do not vary the NLICA algorithm. Additionally, we acknowledge that since contrastive NLICA requires unique assumptions via the positive pair, it is non-trivial to design a task where the assumptions for multiple methods hold, making comparisons challenging. Our method's applicability is limited for inferring weak edges, similar to (Shimizu et al., 2006; Tashiro et al., 2014; Shahbazinia et al., 2021; Lachapelle et al., 2020). As demonstrated in § 5, despite its competitive performance, the success of our proposed method highly relies on the performance of NLICA, which can be limited for higher-dimensional problems. Nonetheless, based on our comparisons, this seems to be an issue for the HSIC independence test as well. A possible

explanation could be that the class of SEMs is harder to learn with specific NLICA algorithms; indeed, we observed that deploying contrastive NLICA (Zimmermann et al., 2021) achieves much better MCC on general (non-triangular) invertible MLPs. To ensure that particular entries in the Jacobian are non-zero everywhere, our assumptions require that the underlying DAG for the DGP is the same for all data points, which might be restrictive . For instance, if the DAG models the interaction of physical objects, then cause-effect relationships are only present when, e.g., the objects are touching each other or their magnetic/electric fields affect each other—in the literature, this setting is considered in (Sontakke et al., 2021; Seitzer et al., 2021).

Unknown causal ordering. Accounting for the causal ordering is, to the best of our knowledge, only found in (Shimizu et al., 2006). Binary CD methods such as (Monti et al., 2019) alleviate this step as they work on an edge-by-edge basis. Other non-ICA-based methods can also avoid this step since the DAG is *invariant* to changes in the causal ordering—meaning that reordering X_i in the observation vector $\boldsymbol{X}$ (cf. Defn. A.11) does not affect the edges of the graph, only their representation in form of an adjacency matrix. However, to resolve the permutation indeterminacy of ICA, we need to account for the causal ordering, since only then can the Jacobian be lower-triangular. Although extracting a lower-triangular Jacobian is easier to interpret and potentially better suited, e.g., as a building block of causal representation learning (since the causal ordering of N_i is always the same), our method extracts the DAG even without resolving these indeterminacies. That is, our demonstration that the permutation indeterminacies can be resolved should mostly be considered as corroboration of Lem. 1.

Extensions to related work. Using neural networks for CD is discussed in several papers (Monti et al., 2019; Khemakhem et al., 2021; Lachapelle et al., 2020; Lippe et al., 2021; 2022; Brouillard et al., 2020), many of them uses the adjacency matrix, the Jacobian of the inference network (Shimizu et al., 2006; Schölkopf et al., 2021; Lachapelle et al., 2020) or that of the score function Rolland et al. (2022). On the other hand, the Jacobian of the generative model is prevalent in the identifiability literature Gresele et al. (2021); Buchholz et al. (2022); Zheng et al. (2022), but they do not make claims about CD. Furthermore, methods that can handle general nonlinear relationships either require interventions (Brouillard et al., 2020; Lippe et al., 2021; 2022) or rely on independence tests (Guo et al., 2022; Monti et al., 2019). Our method was inspired by LiNGAM (Shimizu et al., 2006) to use the Jacobian of the inference network for inferring the DAG and utilizes NLICA (similar to Monti et al. (2019)) to provide theoretical guarantees (Props. 1 and 2) for multivariable CD. Furthermore, we also prove (Lem. 1) and demonstrate (Tab. 1) that the permutation indeterminacy of ICA—and that of an unknown causal ordering—can be resolved in the nonlinear case.

Conclusion. Our method uses the Jacobian of the inference function (mapping from observables to independent variables) and can be thought as a generalization of LiNGAM (Shimizu et al., 2006) to nonlinear Causal Discovery (CD). We prove that the inverse DGP's Jacobian captures the sparsity structure of the DAG (Prop. 1), and show that under strong identifiabilty, the inference model also encodes the same information (Prop. 2). For the latter, we leverage that causal models enable resolving the permutation indeterminacy of ICA under certain assumptions (Lem. 1). We introduced a two-step process to leverage strong identifiability for inferring the DAG of multivariable causal models without constraints on the function class, but assuming non–i.i.d. data. That is, our approach leverages NLICA with auxiliary information (coming from the positive pairs, cf. Ex. 2) for CD. *We do not claim that NLICA is a CD method per se; however, we show that when the underlying generative model can be described by a causal graph and we have non–i.i.d. data, then CD is possible with NLICA.* Particularly, we show that contrastive NLICA (Zimmermann et al., 2021) is compatible with CD. Although the use of the Jacobian is prevalent in the literature, to the best of our knowledge, **we are the first to use the inference model's Jacobian for causal discovery without constraining the function class (but using non–i.i.d. data), while also providing identifiability guarantees**. Since we do not use conditional independence tests, but learn the causal ordering with Sinkhorn networks, our method provides an end-to-end solution for CD and avoids the cost of exponentially many independence tests. We experimentally demonstrate that our proposal can infer the DAG in multiple synthetic data sets.

References

Lazar Atanackovic, Alexander Tong, Jason Hartford, Leo J. Lee, Bo Wang, and Yoshua Bengio. DynGFN: Bayesian Dynamic Causal Discovery using Generative Flow Networks, February 2023. URL `http://arxiv.org/abs/2302.04178`. arXiv:2302.04178 [cs] version: 1. 12, 24, 25

Yoshua Bengio, Tristan Deleu, Nasim Rahaman, Nan Rosemary Ke, Sébastien Lachapelle, Olexa Bilaniuk, Anirudh Goyal, and Christopher J. Pal. A meta-transfer objective for learning to disentangle causal mechanisms. In *8th International Conference on Learning Representations, ICLR 2020, Addis Ababa, Ethiopia, April 26-30, 2020*. OpenReview.net, 2020. 12

Philippe Brouillard, Sébastien Lachapelle, Alexandre Lacoste, Simon Lacoste-Julien, and Alexandre Drouin. Differentiable causal discovery from interventional data. In Hugo Larochelle, Marc'Aurelio Ranzato, Raia Hadsell, Maria-Florina Balcan, and Hsuan-Tien Lin (eds.), *Advances in Neural Information Processing Systems 33: Annual Conference on Neural Information Processing Systems 2020, NeurIPS 2020, December 6-12, 2020, virtual*, 2020. 3, 12, 13, 24

Simon Buchholz, Michel Besserve, and Bernhard Schölkopf. Function classes for identifiable nonlinear independent component analysis. In *Advances in Neural Information Processing Systems*, 2022. 12, 13, 25

Bertrand Charpentier, Simon Kibler, and Stephan Günnemann. Differentiable dag sampling. In *International Conference on Learning Representations*, 2022. 3, 6, 9, 12, 24

Ting Chen, Simon Kornblith, Mohammad Norouzi, and Geoffrey E. Hinton. A simple framework for contrastive learning of visual representations. In *Proceedings of the 37th International Conference on Machine Learning, ICML 2020, 13-18 July 2020, Virtual Event*, volume 119 of *Proceedings of Machine Learning Research*, pp. 1597–1607. PMLR, 2020. 8

Pierre Comon. Independent component analysis, a new concept? *Signal processing*, 36(3):287–314, 1994. 1, 3

George Darmois. Analyse des liaisons de probabilité. In *Proc. Int. Stat. Conferences 1947*, pp. 231, 1951. 3

Yann Dubois, Stefano Ermon, Tatsunori Hashimoto, and Percy Liang. Improving self-supervised learning by characterizing idealized representations. In *Advances in Neural Information Processing Systems*, 2022. 8

Frederick Eberhardt, Clark Glymour, and Richard Scheines. On the number of experiments sufficient and in the worst case necessary to identify all causal relations among n variables. In *Proceedings of the Twenty-First Conference on Uncertainty in Artificial Intelligence*, pp. 178–184, 2005. 1

Élisabeth Gassiat, Sylvain Le Corff, and Luc Lehéricy. Deconvolution with unknown noise distribution is possible for multivariate signals. *Ann. Statist.*, 50(1), February 2022. ISSN 0090-5364. doi: 10.1214/21-aos2106. URL `https://doi.org/10.1214/21-aos2106`. 3

Robert Geirhos, Jörn-Henrik Jacobsen, Claudio Michaelis, Richard Zemel, Wieland Brendel, Matthias Bethge, and Felix A Wichmann. Shortcut learning in deep neural networks. *Nature Machine Intelligence*, 2(11): 665–673, 2020. 1

Olivier Goudet, Diviyan Kalainathan, Philippe Caillou, Isabelle Guyon, David Lopez-Paz, and Michele Sebag. Learning functional causal models with generative neural networks. In *Explainable and interpretable models in computer vision and machine learning*, pp. 39–80. Springer, 2018. 3

Luigi Gresele, Paul K. Rubenstein, Arash Mehrjou, Francesco Locatello, and Bernhard Schölkopf. The Incomplete Rosetta Stone problem: Identifiability results for Multi-view Nonlinear ICA. In *Proceedings of the 35th Conference on Uncertainty in Artificial Intelligence (UAI)*, volume 115 of *Proceedings of Machine Learning Research*, pp. 217–227. PMLR, July 2019. URL `https://proceedings.mlr.press/v115/gresele20a.html`. 2, 3

Luigi Gresele, Julius von Kügelgen, Vincent Stimper, Bernhard Schölkopf, and Michel Besserve. Independent mechanisms analysis, a new concept? In *Advances in Neural Information Processing Systems 34 (NeurIPS 2021)*, pp. 28233–28248. Curran Associates, Inc., December 2021. URL `https://proceedings.neurips.cc/paper/2021/file/edc27f139c3b4e4bb29d1cdbc45663f9-Paper.pdf`. 3, 12, 13, 22, 25

Arthur Gretton, Olivier Bousquet, Alex Smola, and Bernhard Schölkopf. Measuring statistical dependence with Hilbert-Schmidt norms. In Sanjay Jain, Hans Ulrich Simon, and Etsuji Tomita (eds.), *Algorithmic Learning Theory*, Lecture Notes in Computer Science, pp. 63–77, Berlin, Heidelberg, 2005. Springer. ISBN 978-3-540-31696-1. doi: 10.1007/11564089_7. 10

Siyuan Guo, Viktor Tóth, Bernhard Schölkopf, and Ferenc Huszár. Causal de Finetti: On the Identification of Invariant Causal Structure in Exchangeable Data. *ArXiv preprint*, abs/2203.15756, 2022. 1, 3, 7, 8, 11, 13, 24

Hermanni Hälvä and Aapo Hyvärinen. Hidden Markov nonlinear ICA: Unsupervised learning from nonstationary time series. In Ryan P. Adams and Vibhav Gogate (eds.), *Proceedings of the Thirty-Sixth Conference on Uncertainty in Artificial Intelligence, UAI 2020, virtual online, August 3-6, 2020*, volume 124 of *Proceedings of Machine Learning Research*, pp. 939–948. AUAI Press, 2020. 2, 3

Richard Zou Horace He. functorch: Jax-like composable function transforms for pytorch. `https://github.com/pytorch/functorch`, 2021. 9

Patrik O. Hoyer, Dominik Janzing, Joris M. Mooij, Jonas Peters, and Bernhard Schölkopf. Nonlinear Causal Discovery with Additive Noise Models. In Daphne Koller, Dale Schuurmans, Yoshua Bengio, and Léon Bottou (eds.), *Advances in Neural Information Processing Systems 21, Proceedings of the Twenty-Second Annual Conference on Neural Information Processing Systems, Vancouver, British Columbia, Canada, December 8-11, 2008*, pp. 689–696. Curran Associates, Inc., 2008. 1, 3, 4, 5

Antti Hyttinen, Patrik O Hoyer, Frederick Eberhardt, and Matti Järvisalo. Discovering cyclic causal models with latent variables: a general sat-based procedure. In *Proceedings of the Twenty-Ninth Conference on Uncertainty in Artificial Intelligence*, pp. 301–310, 2013. 3

Aapo Hyvärinen and Hiroshi Morioka. Unsupervised Feature Extraction by Time-Contrastive Learning and Nonlinear ICA. In Daniel D. Lee, Masashi Sugiyama, Ulrike von Luxburg, Isabelle Guyon, and Roman Garnett (eds.), *Advances in Neural Information Processing Systems 29: Annual Conference on Neural Information Processing Systems 2016, December 5-10, 2016, Barcelona, Spain*, pp. 3765–3773, 2016. 1, 3, 8

Aapo Hyvärinen and Hiroshi Morioka. Nonlinear ICA of temporally dependent stationary sources. In Aarti Singh and Xiaojin (Jerry) Zhu (eds.), *Proceedings of the 20th International Conference on Artificial Intelligence and Statistics, AISTATS 2017, 20-22 April 2017, Fort Lauderdale, FL, USA*, volume 54 of *Proceedings of Machine Learning Research*, pp. 460–469. PMLR, 2017. 2, 3, 8, 22

Aapo Hyvärinen and Petteri Pajunen. Nonlinear Independent Component Analysis: Existence and Uniqueness Results. *Neural Networks*, 12(3):429–439, April 1999. ISSN 0893-6080. doi: 10.1016/s0893-6080(98)00140-3. URL `https://doi.org/10.1016/s0893-6080(98)00140-3`. 3, 7

Aapo Hyvärinen, Juha Karhunen, and Erkki Oja. *Independent Component Analysis*. John Wiley & Sons, Inc., New York, May 2001. ISBN 047140540X, 0471221317. doi: 10.1002/0471221317. URL `https://doi.org/10.1002/0471221317`. 1, 3, 5

Aapo Hyvärinen, Kun Zhang, Shohei Shimizu, and Patrik O Hoyer. Estimation of a Structural Vector Autoregression Model Using Non-Gaussianity. *Journal of Machine Learning Research*, 11(5), 2010. 2, 3

Aapo Hyvärinen, Hiroaki Sasaki, and Richard E. Turner. Nonlinear ICA Using Auxiliary Variables and Generalized Contrastive Learning. In Kamalika Chaudhuri and Masashi Sugiyama (eds.), *The 22nd International Conference on Artificial Intelligence and Statistics, AISTATS 2019, 16-18 April 2019, Naha, Okinawa, Japan*, volume 89 of *Proceedings of Machine Learning Research*, pp. 859–868. PMLR, 2019. 1, 3

Aapo Hyvärinen, Ilyes Khemakhem, and Ricardo Monti. Identifiability of latent-variable and structural-equation models: from linear to nonlinear, February 2023. URL `http://arxiv.org/abs/2302.02672`. arXiv:2302.02672 [cs, stat]. 3, 22

Dominik Janzing, Jonas Peters, Joris Mooij, and Bernhard Schölkopf. Identifying confounders using additive noise models. In *Proceedings of the Twenty-Fifth Conference on Uncertainty in Artificial Intelligence*, pp. 249–257, 2009. 11

Diviyan Kalainathan, Olivier Goudet, Isabelle Guyon, David Lopez-Paz, and Michèle Sebag. Structural Agnostic Modeling: Adversarial Learning of Causal Graphs. *ArXiv preprint*, abs/1803.04929, 2018. 3, 12, 24

Rickard K. A. Karlsson and Jesse H. Krijthe. Combining observational datasets from multiple environments to detect hidden confounding, May 2022. URL http://arxiv.org/abs/2205.13935. arXiv:2205.13935 [cs, stat]. 11

Nan Rosemary Ke, Olexa Bilaniuk, Anirudh Goyal, Stefan Bauer, Hugo Larochelle, Bernhard Schölkopf, Michael C. Mozer, Chris Pal, and Yoshua Bengio. Learning Neural Causal Models from Unknown Interventions. *arXiv:1910.01075 [cs, stat]*, August 2020. URL http://arxiv.org/abs/1910.01075. arXiv: 1910.01075. 3, 9, 12, 24

Ilyes Khemakhem, Diederik P. Kingma, Ricardo Pio Monti, and Aapo Hyvärinen. Variational Autoencoders and Nonlinear ICA: A Unifying Framework. In Silvia Chiappa and Roberto Calandra (eds.), *The 23rd International Conference on Artificial Intelligence and Statistics, AISTATS 2020, 26-28 August 2020, Online [Palermo, Sicily, Italy]*, volume 108 of *Proceedings of Machine Learning Research*, pp. 2207–2217. PMLR, 2020a. 1, 3, 5

Ilyes Khemakhem, Ricardo Pio Monti, Diederik P. Kingma, and Aapo Hyvärinen. ICE-BeeM: Identifiable conditional energy-based deep models based on nonlinear ICA. In Hugo Larochelle, Marc'Aurelio Ranzato, Raia Hadsell, Maria-Florina Balcan, and Hsuan-Tien Lin (eds.), *Advances in Neural Information Processing Systems 33: Annual Conference on Neural Information Processing Systems 2020, NeurIPS 2020, December 6-12, 2020, virtual*, 2020b. 1, 2, 21, 22

Ilyes Khemakhem, Ricardo Pio Monti, Robert Leech, and Aapo Hyvärinen. Causal Autoregressive Flows. In Arindam Banerjee and Kenji Fukumizu (eds.), *The 24th International Conference on Artificial Intelligence and Statistics, AISTATS 2021, April 13-15, 2021, Virtual Event*, volume 130 of *Proceedings of Machine Learning Research*, pp. 3520–3528. PMLR, 2021. 3, 12, 13, 22, 24

David A. Klindt, Lukas Schott, Yash Sharma, Ivan Ustyuzhaninov, Wieland Brendel, Matthias Bethge, and Dylan M. Paiton. Towards nonlinear disentanglement in natural data with temporal sparse coding. In *9th International Conference on Learning Representations, ICLR 2021, Virtual Event, Austria, May 3-7, 2021*. OpenReview.net, 2021. 1, 3, 8

Andrej N Kolmogorov. Sulla determinazione empirica di una legge didistribuzione. *Giorn Dell'inst Ital Degli Att*, 4:89–91, 1933. 27

Harold W Kuhn. The hungarian method for the assignment problem. *Naval research logistics quarterly*, 2 (1-2):83–97, 1955. 10

Trent Kyono, Yao Zhang, and Mihaela van der Schaar. Castle: Regularization via auxiliary causal graph discovery. *Advances in Neural Information Processing Systems*, 33:1501–1512, 2020. 3

Sébastien Lachapelle, Philippe Brouillard, Tristan Deleu, and Simon Lacoste-Julien. Gradient-based neural DAG learning. In *8th International Conference on Learning Representations, ICLR 2020, Addis Ababa, Ethiopia, April 26-30, 2020*. OpenReview.net, 2020. 1, 3, 9, 12, 13, 24, 25

Sébastien Lachapelle, Pau Rodriguez, Yash Sharma, Katie E Everett, Rémi Le Priol, Alexandre Lacoste, and Simon Lacoste-Julien. Disentanglement via mechanism sparsity regularization: A new principle for nonlinear ica. In *Conference on Causal Learning and Reasoning*, pp. 428–484. PMLR, 2022. 2

Hao-Chih Lee, Matteo Danieletto, Riccardo Miotto, Sarah T Cherng, and Joel T Dudley. Scaling structural learning with no-bears to infer causal transcriptome networks. In *PACIFIC SYMPOSIUM ON BIOCOMPUTING 2020*, pp. 391–402. World Scientific, 2019. 3

Phillip Lippe, Taco Cohen, and Efstratios Gavves. Efficient neural causal discovery without acyclicity constraints. *ArXiv preprint*, abs/2107.10483, 2021. 3, 12, 13, 24

Phillip Lippe, Sara Magliacane, Sindy Löwe, Yuki M Asano, Taco Cohen, and Stratis Gavves. CITRIS: Causal Identifiability from Temporal Intervened Sequences. In *International Conference on Machine Learning*, pp. 13557–13603. PMLR, 2022. 12, 13

Francesco Locatello, Stefan Bauer, Mario Lucic, Gunnar Rätsch, Sylvain Gelly, Bernhard Schölkopf, and Olivier Bachem. Challenging common assumptions in the unsupervised learning of disentangled representations. In Kamalika Chaudhuri and Ruslan Salakhutdinov (eds.), *Proceedings of the 36th International Conference on Machine Learning, ICML 2019, 9-15 June 2019, Long Beach, California, USA*, volume 97 of *Proceedings of Machine Learning Research*, pp. 4114–4124. PMLR, 2019. 3

Lars Lorch, Jonas Rothfuss, Bernhard Schölkopf, and Andreas Krause. DiBS: Differentiable Bayesian Structure Learning. *Advances in Neural Information Processing Systems*, 34:24111–24123, 2021. 3, 12, 24, 25

Lars Lorch, Scott Sussex, Jonas Rothfuss, Andreas Krause, and Bernhard Schölkopf. Amortized inference for causal structure learning. In *NeurIPS 2022 Workshop on Causality for Real-world Impact*, 2022. 2, 3, 12, 24

Ian D. Macdonald. *The theory of groups / Ian D. Macdonald*. Clarendon Press Oxford, 1968. ISBN 0198531389. 23

Gonzalo E. Mena, David Belanger, Scott W. Linderman, and Jasper Snoek. Learning latent permutations with gumbel-sinkhorn networks. In *6th International Conference on Learning Representations, ICLR 2018, Vancouver, BC, Canada, April 30 - May 3, 2018, Conference Track Proceedings*. OpenReview.net, 2018. 6, 9, 29

Jovana Mitrovic, Dino Sejdinovic, and Yee Whye Teh. Causal inference via kernel deviance measures. *Advances in neural information processing systems*, 31, 2018. 3

Ricardo Pio Monti, Kun Zhang, and Aapo Hyvärinen. Causal discovery with general non-linear relationships using non-linear ICA. In Amir Globerson and Ricardo Silva (eds.), *Proceedings of the Thirty-Fifth Conference on Uncertainty in Artificial Intelligence, UAI 2019, Tel Aviv, Israel, July 22-25, 2019*, volume 115 of *Proceedings of Machine Learning Research*, pp. 186–195. AUAI Press, 2019. 1, 2, 3, 8, 9, 10, 11, 13, 22, 24

Raha Moraffah, Bahman Moraffah, Mansooreh Karami, Adrienne Raglin, and Huan Liu. Causal adversarial network for learning conditional and interventional distributions. *ArXiv preprint*, abs/2008.11376, 2020. 3

Hiroshi Morioka, Hermanni Hälvä, and Aapo Hyvärinen. Independent innovation analysis for nonlinear vector autoregressive process. In Arindam Banerjee and Kenji Fukumizu (eds.), *The 24th International Conference on Artificial Intelligence and Statistics, AISTATS 2021, April 13-15, 2021, Virtual Event*, volume 130 of *Proceedings of Machine Learning Research*, pp. 1549–1557. PMLR, 2021. 1, 3, 8

Ignavier Ng, AmirEmad Ghassami, and Kun Zhang. On the Role of Sparsity and DAG Constraints for Learning Linear DAGs. *Advances in Neural Information Processing Systems*, 33:17943–17954, 2020. 3

Ignavier Ng, Shengyu Zhu, Zhuangyan Fang, Haoyang Li, Zhitang Chen, and Jun Wang. Masked Gradient-Based Causal Structure Learning. In *Proceedings of the 2022 SIAM International Conference on Data Mining (SDM)*, pp. 424–432. SIAM, 2022. 1, 3, 12, 24

Adam Paszke, Sam Gross, Francisco Massa, Adam Lerer, James Bradbury, Gregory Chanan, Trevor Killeen, Zeming Lin, Natalia Gimelshein, Luca Antiga, et al. Pytorch: An imperative style, high-performance deep learning library. *Advances in neural information processing systems*, 32, 2019. 9

Judea Pearl. *Causality*. Cambridge University Press, Cambridge, 2 edition, September 2009. ISBN 9780511803161, 9780521895606, 9780521749190. doi: 10.1017/cbo9780511803161. URL `https://doi.org/10.1017/cbo9780511803161`. 2, 3, 7, 11

J Peters, J Mooij, D Janzing, and B Schölkopf. Identifiability of causal graphs using functional models. In FG Cozman and A Pfeffer (eds.), *27th Conference on Uncertainty in Artificial Intelligence (UAI 2011)*, pp. 589–598, Corvallis, OR, USA, 2011. AUAI Press. 1, 4

J. Peters, D. Janzing, and B. Schölkopf. *Elements of Causal Inference – Foundations and Learning Algorithms*. MIT Press, Cambridge, MA, USA, 2017. 1, 3, 11, 20

Garvesh Raskutti and Caroline Uhler. Learning directed acyclic graph models based on sparsest permutations. *Stat*, 7(1):e183, 2018. 3

Paul Rolland, Volkan Cevher, Matthäus Kleindessner, Chris Russell, Dominik Janzing, Bernhard Schölkopf, and Francesco Locatello. Score Matching Enables Causal Discovery of Nonlinear Additive Noise Models. In *International Conference on Machine Learning*, pp. 18741–18753. PMLR, 2022. 12, 13, 24, 25

Bernhard Schölkopf, Francesco Locatello, Stefan Bauer, Nan Rosemary Ke, Nal Kalchbrenner, Anirudh Goyal, and Yoshua Bengio. Toward causal representation learning. *Proc. IEEE*, 109(5):612–634, May 2021. ISSN 0018-9219, 1558-2256. doi: 10.1109/jproc.2021.3058954. URL `https://doi.org/10.1109/jproc.2021.3058954`. 1, 3, 12, 13, 24

Maximilian Seitzer, Bernhard Schölkopf, and Georg Martius. Causal influence detection for improving efficiency in reinforcement learning. *Advances in Neural Information Processing Systems*, 34:22905–22918, 2021. 13

Amirhossein Shahbazinia, Saber Salehkaleybar, and Matin Hashemi. ParaLiNGAM: Parallel causal structure learning for linear non-gaussian acyclic models. *arXiv: Distributed, Parallel, and Cluster Computing*, 2021. DOI:, MAG ID: 3202634766. 1, 12

Xinwei Shen, Furui Liu, Hanze Dong, Qing Lian, Zhitang Chen, and Tong Zhang. Weakly Supervised Disentangled Generative Causal Representation Learning. *Journal of Machine Learning Research*, 23:1–55, 2022. 1, 3, 24

Shohei Shimizu, Patrik O Hoyer, Aapo Hyvärinen, Antti Kerminen, and Michael Jordan. A Linear Non-Gaussian Acyclic Model for Causal Discovery. *Journal of Machine Learning Research*, 7(10), 2006. 1, 2, 3, 4, 5, 6, 11, 12, 13, 22, 24, 25

Nickolay Smirnov. Table for estimating the goodness of fit of empirical distributions. *The annals of mathematical statistics*, 19(2):279–281, 1948. 27

Sumedh A. Sontakke, Arash Mehrjou, Laurent Itti, and Bernhard Schölkopf. Causal curiosity: RL agents discovering self-supervised experiments for causal representation learning. In Marina Meila and Tong Zhang (eds.), *Proceedings of the 38th International Conference on Machine Learning, ICML 2021, 18-24 July 2021, Virtual Event*, volume 139 of *Proceedings of Machine Learning Research*, pp. 9848–9858. PMLR, 2021. 13

Peter Spirtes and Kun Zhang. Causal discovery and inference: Concepts and recent methodological advances. *Applied Informatics*, 3(1):3, February 2016. ISSN 2196-0089. doi: 10.1186/s40535-016-0018-x. URL `https://doi.org/10.1186/s40535-016-0018-x`. 11

Peter Spirtes, Clark N Glymour, Richard Scheines, and David Heckerman. *Causation, prediction, and search*. MIT press, 2000. 3, 11

Chandler Squires, Anna Seigal, Salil Bhate, and Caroline Uhler. Linear Causal Disentanglement via Interventions, February 2023. URL `http://arxiv.org/abs/2211.16467`. arXiv:2211.16467 [cs, stat]. 3, 24

Mikhail Fedorovich Subbotin. On the law of frequency of error. *Mat. Sb.*, 31(2):296–301, 1923. 8

Tatsuya Tashiro, Shohei Shimizu, Aapo Hyvärinen, and Takashi Washio. ParceLiNGAM: A causal ordering method robust against latent confounders. *Neural Comput.*, 26(1):57–83, January 2014. ISSN 0899-7667, 1530-888X. doi: 10.1162/neco_a_00533. URL `https://doi.org/10.1162/neco_a_00533`. 1, 12

Ashish Vaswani, Noam Shazeer, Niki Parmar, Jakob Uszkoreit, Llion Jones, Aidan N Gomez, Łukasz Kaiser, and Illia Polosukhin. Attention is all you need. *Advances in neural information processing systems*, 30, 2017. 12

Julius Von Kügelgen, Yash Sharma, Luigi Gresele, Wieland Brendel, Bernhard Schölkopf, Michel Besserve, and Francesco Locatello. Self-Supervised Learning with Data Augmentations Provably Isolates Content from Style. *Advances in neural information processing systems*, 34:16451–16467, 2021. 3, 22

Matthew J. Vowels, Necati Cihan Camgoz, and Richard Bowden. D'ya like DAGs? a survey on structure learning and causal discovery. *ACM Comput. Surv.*, abs/2103.02582, April 2022. ISSN 0360-0300, 1557-7341. doi: 10.1145/3527154. URL `https://doi.org/10.1145/3527154`. 3, 9

Dennis Wei, Tian Gao, and Yue Yu. Dags with no fears: A closer look at continuous optimization for learning bayesian networks. *Advances in Neural Information Processing Systems*, 33:3895–3906, 2020. 3

Matthew Willetts and Brooks Paige. I Don't Need $\mathbf{u}$: Identifiable Non-Linear ICA Without Side Information. *ArXiv preprint*, abs/2106.05238, 2021. 1

Mengyue Yang, Furui Liu, Zhitang Chen, Xinwei Shen, Jianye Hao, and Jun Wang. CausalVAE: Disentangled Representation Learning via Neural Structural Causal Models. In *2021 IEEE/CVF Conference on Computer Vision and Pattern Recognition (CVPR)*, pp. 9588–9597, 2021. doi: 10.1109/CVPR46437.2021.00947. 3, 24

Yue Yu, Jie Chen, Tian Gao, and Mo Yu. DAG-GNN: Dag structure learning with graph neural networks. In Kamalika Chaudhuri and Ruslan Salakhutdinov (eds.), *Proceedings of the 36th International Conference on Machine Learning, ICML 2019, 9-15 June 2019, Long Beach, California, USA*, volume 97 of *Proceedings of Machine Learning Research*, pp. 7154–7163. PMLR, 2019. 1, 3, 12, 24

K Zhang and A Hyvärinen. On the Identifiability of the Post-Nonlinear Causal Model. In *25th Conference on Uncertainty in Artificial Intelligence (UAI 2009)*, pp. 647–655. AUAI Press, 2009. 3

Kun Zhang, Jiji Zhang, and Bernhard Schölkopf. Distinguishing Cause from Effect Based on Exogeneity. In *Fifteenth Conference on Theoretical Aspects of Rationality and Knowledge (TARK), 2015*, pp. 261–271. Carnegie Mellon University, 2015. 1, 3

Xun Zheng, Bryon Aragam, Pradeep Ravikumar, and Eric P. Xing. DAGs with NO TEARS: Continuous optimization for structure learning. In Samy Bengio, Hanna M. Wallach, Hugo Larochelle, Kristen Grauman, Nicolò Cesa-Bianchi, and Roman Garnett (eds.), *Advances in Neural Information Processing Systems 31: Annual Conference on Neural Information Processing Systems 2018, NeurIPS 2018, December 3-8, 2018, Montréal, Canada*, pp. 9492–9503, 2018. 1, 3, 12, 24

Yujia Zheng, Ignavier Ng, and Kun Zhang. On the identifiability of nonlinear ica: Sparsity and beyond. In *Advances in Neural Information Processing Systems*, 2022. 12, 13, 24, 25

Roland S. Zimmermann, Yash Sharma, Steffen Schneider, Matthias Bethge, and Wieland Brendel. Contrastive learning inverts the data generating process. In Marina Meila and Tong Zhang (eds.), *Proceedings of the 38th International Conference on Machine Learning, ICML 2021, 18-24 July 2021, Virtual Event*, volume 139 of *Proceedings of Machine Learning Research*, pp. 12979–12990. PMLR, 2021. 1, 3, 5, 7, 8, 9, 10, 13, 22, 23

Appendix

A SEMs

Definition A.1 (SEM)**.** *A SEM describes causal relationships via a set of structural assignments (Peters et al., 2017):*

$$X_i := f_i\left(\boldsymbol{Pa}_i, N_i\right), \qquad \forall i \in \mathcal{I} = \{1, \ldots, d\}, \tag{7}$$

where X_i are the endogenous, N_i the exogenous/noise variables, $\boldsymbol{Pa}_i \subseteq \boldsymbol{X} \setminus \{X_i\}$ denotes the parent set of X_i, $\mathcal{I}$ the set of indices, and f_i the mappings.

Definition A.2 (Reduced form of SEM)**.** *The reduced form of the SEM expresses all X_i as a function of only the N_i variables, i.e.:*

$$X_i := f_i\left(\boldsymbol{N}^i\right), \qquad \forall i \in \mathcal{I} = \{0, \ldots, d-1\}, \tag{8}$$

with the same notation as in Defn. A.1, slightly abusing f_i and denoting a subset of $\boldsymbol{N}$ by $\boldsymbol{N}^i \subseteq \boldsymbol{N}$.

Definition A.3 (Chain)**.** *A graphical structure of three nodes X_k, X_p, X_q is called a chain if two nodes are both parents of the third. Graphically, this means:*

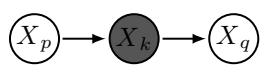

Figure 5: Visualization of a chain. Conditioning on the middle node (denoted with gray color) blocks the path $X_p \to X_k \to X_q$.

That is, the following conditional independence (denoted by $\perp$) relationship holds:

$$X_p \perp X_q | X_k \tag{9}$$

Definition A.4 (Collider)**.** *A graphical structure of three nodes X_k, X_p, X_q is called a collider if two nodes are both parents of the third. Graphically, this means:*

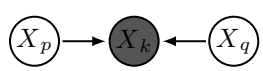

Figure 6: Visualization of a collider. Conditioning on the collider node (denoted with gray color) opens the path $X_p \to X_k \leftarrow X_q$.

That is, the following conditional dependence (denoted by $\not\perp$) relationship holds:

$$X_p \not\perp X_q | X_k \tag{10}$$

Definition A.5 (Fork)**.** *A graphical structure of three nodes X_k, X_p, X_q is called a fork if one node is the parent of the two other nodes. Graphically, this means:*

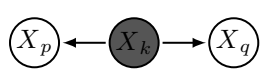

Figure 7: Visualization of a fork. Conditioning on the fork node (denoted with gray color) blocks the path $X_p \leftarrow X_k \to X_q$.

That is, the following conditional independence (denoted by $\perp$) relationship holds:

$$X_p \perp X_q | X_k \tag{11}$$

Definition A.6 (Confounder (unobserved common cause))**.** *In a DAG with nodes $X_i : \forall i \in \mathcal{I} = \{1, \dots, d\}$ a node X_k is called a confounder if there exist at least two $p, q \in \mathcal{I} : X_k \in \boldsymbol{Pa}_p \wedge X_k \in \boldsymbol{Pa}_q$ and X_k is unobserved. Graphically,*

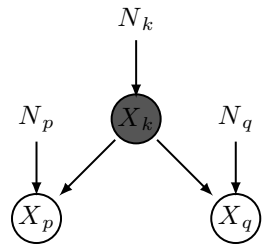

Figure 8: Visualization of a confounder (unobserved common cause), indicated by a gray node color.

Definition A.7 (Causal ordering)**.** *The causal ordering π is a bijective automorphism on the index set $\mathcal{I}$. Namely, $\pi : \mathcal{I} \to \mathcal{I}$ so that $\forall X_i \neq X_j$, it holds that if $\pi(i) < \pi(j) \implies X_j \notin \boldsymbol{Pa}_i$.*

The definition means that only a node with a smaller index in π can be a parent of a node with a larger index. Note that though X_i *can* be a parent of X_j, it is not necessary, but X_j *cannot* be a parent of X_i. Multiple orderings may exist, e.g. if there are multiple X_i so that they only have a single parent. π helps to have a unique description of the edges in the graph. Namely, if the edges are organized in the adjacency matrix $\boldsymbol{\mathcal{A}}$ according to π, then $\boldsymbol{\mathcal{A}}$ will be strictly lower triangular.

Definition A.8 (Adjacency matrix)**.** *The adjacency matrix $\boldsymbol{\mathcal{A}}$ is a binary $d \times d$ matrix, where $\boldsymbol{\mathcal{A}}_{ij} = 1 \iff X_j \in \boldsymbol{Pa}_i$. The rows of $\boldsymbol{\mathcal{A}}$ are ordered by π; thus, $\boldsymbol{\mathcal{A}}$ is strictly lower-triangular.*

$\boldsymbol{\mathcal{A}}$ only describes the edges of the DAG, which gives the direct cause-effect relationships. Nodes can be influence each other via paths (i.e., a set of directed edges that can be traversed between the two nodes), which can be described by the connectivity matrix $\boldsymbol{\mathcal{C}}$

Definition A.9 (Connectivity matrix)**.** *The connectivity matrix $\boldsymbol{\mathcal{C}}$ is a binary $d \times d$ matrix, where $\boldsymbol{\mathcal{C}} = 1 \iff \exists p : X_j \to \dots \to X_i$. $\boldsymbol{\mathcal{C}} = \sum_{k=1}^{d} \boldsymbol{\mathcal{A}}^k$. The rows of $\boldsymbol{\mathcal{C}}$ are ordered by π; thus, $\boldsymbol{\mathcal{C}}$ is strictly lower-triangular.*

Assumption A.1 (Structural faithfulness)**.** *The set of $\boldsymbol{N}$'s that induces additional zeroes (i.e., a sparser DAG) in the Jacobians $\mathbf{J}_{\boldsymbol{f}}$, $\mathbf{J}_{\boldsymbol{f}^{-1}}$ has zero measure, i.e., both Jacobians describe the sparsity structure of the underlying DAG DGP with probability one ($\mathbf{J}_{\boldsymbol{f}}$ w.r.t. $\boldsymbol{\mathcal{C}}$, as shown in Lem. A.1; $\mathbf{J}_{\boldsymbol{f}^{-1}}$ w.r.t. $\boldsymbol{\mathcal{A}}$). Alternatively, the structural independencies are reflected in a functional form via $\mathbf{J}_{\boldsymbol{f}}/\mathbf{J}_{\boldsymbol{f}^{-1}}$. We call this property structural faithfulness.*

Definition A.10 (DGP with known π)**.** *The DGP is described by the SEM, when π is known. I.e., the flow of information is: $\boldsymbol{N} \xrightarrow{SEM} \boldsymbol{X}$.*

Definition A.11 (DGP with unknown π)**.** *The DGP with unknown π is given by the SEM, and by a permutation matrix π (with a slight abuse of notation) applied to $\boldsymbol{X}$. I.e., the flow of information is: $\boldsymbol{N} \xrightarrow{SEM} \boldsymbol{X} \xrightarrow{\pi} \hat{\boldsymbol{X}}$.*

Lemma A.1 ($\mathbf{J}_{\boldsymbol{f}} \sim_{DAG} (\mathbf{I}_d + \boldsymbol{\mathcal{C}})$)**.** *Given Assum. 1, the partial derivatives of f_i w.r.t. N_j provide information about $\boldsymbol{\mathcal{C}}$, as*

$$(\mathbf{J}_{\boldsymbol{f}})_{kl} = \frac{\partial f_l}{\partial N_k} = 0 \iff \nexists X_k \to \dots \to X_l$$

We emphasize that the derivatives are also non-zero in the case of indirect paths, i.e., when $\exists X_i \in p : i \neq k, l$. Furthermore, the strictly lower triangular part of $\mathbf{J}_{\boldsymbol{f}}$ has the describes the same DAG as $\boldsymbol{\mathcal{C}}$–or equivalently, $\mathbf{J}_{\boldsymbol{f}} \sim_{DAG} (\mathbf{I}_d + \boldsymbol{\mathcal{C}})$.

B Identifiability definitions

Definition B.1 (Strong Identifiability (Khemakhem et al., 2020b))**.** *Given a parameter class Θ, when the feature extractors $\boldsymbol{g}_{\theta_1}, \boldsymbol{g}_{\theta_2} : \mathcal{X} \to \mathcal{N}$ produce latent representations $\boldsymbol{N}_1 = \boldsymbol{g}_{\theta_1}(\boldsymbol{X}), \boldsymbol{N}_2 = \boldsymbol{g}_{\theta_2}(\boldsymbol{X})$ that are*

equivalent up to scaled permutations and offsets c for all $\theta_1, \theta_2 \in \Theta$, i.e.,

$$\theta_1 \sim \theta_2 \iff \boldsymbol{N} = \boldsymbol{g}_{\theta_1}(\boldsymbol{X}) = \mathbf{D}\mathbf{P}\boldsymbol{g}_{\theta_2}(\boldsymbol{X}) + c, \tag{12}$$

where $\mathbf{D}$ *is a diagonal and* $\mathbf{P}$ *a permutation matrix. Then* θ_1, θ_2 *fulfill an equivalence relationship.*

Definition B.2 (Weak Identifiability (Khemakhem et al., 2020b))**.** *Given a parameter class* Θ*, when the feature extractors* $\boldsymbol{g}_{\theta_1}, \boldsymbol{g}_{\theta_2} : \mathcal{X} \to \mathcal{N}$ *produce latent representations* $\boldsymbol{N}_1 = \boldsymbol{g}_{\theta_1}(\boldsymbol{X}), \boldsymbol{N}_2 = \boldsymbol{g}_{\theta_2}(\boldsymbol{X})$ *that are equivalent up to matrix multiplications and offsets* c *for all* $\theta_1, \theta_2 \in \Theta$*, i.e.,*

$$\theta_1 \sim \theta_2 \iff \boldsymbol{N} = \boldsymbol{g}_{\theta_1}(\boldsymbol{X}) = \mathbf{A}\boldsymbol{g}_{\theta_2}(\boldsymbol{X}) + c, \tag{13}$$

where $\operatorname{rank}(\mathbf{A}) \geq \min(\dim \mathcal{N}; \dim \mathcal{X})$*. Then* θ_1, θ_2 *fulfill an equivalence relationship.*

Definition B.3 (Identifiability up to elementwise nonlinearities (Hyvärinen & Morioka, 2017))**.** *Given a parameter class* Θ*, when the feature extractors* $\boldsymbol{g}_{\theta_1}, \boldsymbol{g}_{\theta_2} : \mathcal{X} \to \mathcal{N}$ *produce latent representations* $\boldsymbol{N}_1 = \boldsymbol{g}_{\theta_1}(\boldsymbol{X}), \boldsymbol{N}_2 = \boldsymbol{g}_{\theta_2}(\boldsymbol{X})$ *that are equivalent up to elementwise nonlinearities, matrix multiplications and offsets* c *for all* $\theta_1, \theta_2 \in \Theta$*, i.e.,*

$$\theta_1 \sim \theta_2 \iff \boldsymbol{N} = \boldsymbol{g}_{\theta_1}(\boldsymbol{X}) = \mathbf{A}\sigma\left[\boldsymbol{g}_{\theta_2}(\boldsymbol{X})\right] + c, \tag{14}$$

where $\operatorname{rank}(\mathbf{A}) \geq \min(\dim \mathcal{N}; \dim \mathcal{X})$ *and* σ *denotes an elementwise nonlinear transformation. Then* θ_1, θ_2 *fulfill an equivalence relationship.*

C Compatibility of SEM–ICA assumptions

Several works investigated the relationship between SEM and ICA (Gresele et al., 2021; Monti et al., 2019; Shimizu et al., 2006; Von Kügelgen et al., 2021; Hyvärinen et al., 2023); however, it is unclear whether and which assumptions of both fields are compatible. This section relies on (Monti et al., 2019, App. B.), where the authors detail the SEM–ICA connection for linear models. The clear difference is that the conventional SEM formulation (Defn. A.1) expresses each X_i as a function of $\boldsymbol{Pa}_i$and N_i; whereas ICA only uses N_i. Formally:

$$X_i := f_i(\boldsymbol{Pa}_i, N_i), \qquad \forall i \in \mathcal{I} = \{, \ldots, d\} \tag{15}$$

$$X_i := f_i^*\left(\boldsymbol{N}^i\right), \qquad \forall i \in \mathcal{I} = \{0, \ldots, d-1\}, \tag{16}$$

where the former is the conventional definition (Defn. A.1), whereas the latter is a reduced form of the SEM (Defn. A.2, with $\boldsymbol{N}^i$ denoting a subset of $\boldsymbol{N}$, i.e., $\boldsymbol{N}^i \subseteq \boldsymbol{N}$), corresponding to the ICA model. Note that we use an asterisk to denote that the f_i of the two equations *can be different.*

C.1 Bijectivity of f

It is common to assume a *bijective* map from the causes (sources) to the effects (observations) in both the causality (Khemakhem et al., 2021; Gresele et al., 2021; Monti et al., 2019) and the ICA (Zimmermann et al., 2021; Von Kügelgen et al., 2021; Shimizu et al., 2006; Gresele et al., 2021) literatures. However, since the maps in (15) and (16) are not necessarily the same, we need to investigate whether those assumptions are compatible.

Proposition 3 (Equivalence of bijectivity in SEMs and ICA)**.** *Assuming bijectivity of* $f_i(\boldsymbol{Pa}_i, N_i)$ *and that of* $f_i^*\left(\boldsymbol{N}^i\right)$ *are equivalent.*

Proof. For the proof, we will use an inductive argument and, w.l.o.g., assume that each X_i depends on all $N_{j \leq i}$ (if there are less dependencies, those arguments can be omitted).

$f_i \implies f_i^*$ We start from the conventional SEM equations (Defn. A.1):

$$X_1 := f_1(N_1) \tag{17}$$

$$X_2 := f_2(X_1, N_2) \tag{18}$$

Visually, the question is whether the blue and the red arrows commute (blue are assumed to be bijective, the red's bijectivty needs to be proven):

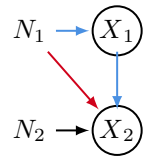

By assumption, f_1 is bijective (in N_1), and so is f_2 (in X_1 and N_2). Since $f_1 \equiv f_1^*$, we proceed to (18) and substitute (17) into (18), yielding:

$$X_2 := f_2\left(f_1\left(N_1\right), N_2\right). \tag{19}$$

Since the composition of bijective maps is bijective (Macdonald, 1968), so the map from N_1 to X_2 is bijective, since the maps $N_1 \to X_1$ and $X_1 \to X_2$ are bijective by assumption, yielding the bijectivity of f_i^*. Then, we apply the same argument inductively for $X_3 := f_2\left(X_1, X_2, N_3\right)$, and up to X_d.

$f_i \Longleftarrow f_i^*$ We start from the reduced SEM equations (Defn. A.2):

$$X_1 := f_1^*\left(N_1\right) \tag{20}$$
$$X_2 := f_2^*\left(N_1, N_2\right). \tag{21}$$

Visually, the question is whether the blue and the red arrows commute (blue are assumed to be bijective, the red's bijectivty needs to be proven):

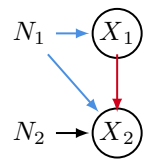

By assumption, f_1^* is bijective (in N_1), and so is f_2^* (in N_1 and N_2). Again, $f_1 \equiv f_1^*$, so we proceed to (21). Since X_1 and N_1 relate via a bijective map, there is no information lost in the mapping. Thus, using X_1 instead of N_1 is possible since f_1^* maintains bijectivity—it can be undone by $\left(f_1^*\right)^{-1}$, which exists by assumption. $N_1 \to X_1$ and $N_1 \to X_2$ are bijective maps, decomposing the latter into $N_1 \to X_1 \to X_2$ only implies that $N_1 \to X_1$ is injective and $X_1 \to X_2$ is surjective (Macdonald, 1968). Fortunately, the $N_1 \to X_1$ is bijective by assumption, so we only need to show that $X_1 \to X_2$ is not only surjective, but also bijective. Since both X_1 and X_2 have the same domain, $X_1 \to X_2$ is bijective (Macdonald, 1968). Then, we apply the same argument inductively for $X_3 := f_2\left(N_1, N_2, N_3\right)$, and up to X_d. □

C.2 Does identifiability imply no confounders?

Identifiabilty can be thought of as "inverting" the DGP Zimmermann et al. (2021). So the question is whether identifiability implies that the learned representation needs to capture all N_i, when the assumptions include that N_i are *jointly independent*? Additionally, we assume that $\dim \boldsymbol{N} = \dim \boldsymbol{X} = d$. Intuitively, if there would be a confounder, it would induce *additional*[5] correlation between at least two X_p and X_q. That is, N_p and N_q would need to "emulate" that when X_k changes (via N_k), then both X_p and X_q would need to change.

Proposition 4 (Identifying jointly independent N_i implies no confounders.)**.** *Under the assumption of jointly independent N_i and $\dim \boldsymbol{N} = \dim \boldsymbol{X} = d$, identifiability at least up to elementwise nonlinearities (Defn. B.3) implies that there cannot be confounders.*

Proof. We assume that there is a confounder X_k, which is the common cause of X_p and X_q—the argument generalizes to more children of X_k. Two cases emerge: when there is a directed path $X_p \to \cdots \to X_q$ (p and q are interchangeable for our argument), or when there is none.

[5]That is, X_p can be the parent of X_q, and they still can have another common cause X_k

No directed path between X_p and X_q Recall from Defn. A.6 that these relationships materialize in the following graph:

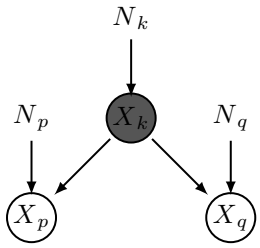

Figure 9: Visualization of a confounder (unobserved common cause), indicated by a gray node color.

From the graph, we can describe the conditional independence relationship of N_p and N_q. Namely, we have access to observations X_p and X_q, implying ($\perp$ denotes conditional independence):

$$N_p \not\perp N_q | X_p, X_q \quad , \tag{22}$$

since conditioning of X_p and X_q activates the colliders (Defn. A.4) $N_p \to X_p \leftarrow X_k$ and $X_k \to X_q \leftarrow N_q$, the path between N_p and N_q opens up. Thus, N_p and N_q become dependent, contradicting the assumption that $N_p \perp N_q$.

There is at least one directed path between X_p and X_q By noticing that conditioning on X_p and X_q blocks any paths between X_p and X_q, the conclusion is the same as above. □

D Extended related work

Table 4: Comparison of CD methods. Column $\mathbf{x}$ indicates multivariability, $do(\emptyset)$ indicates whether the method can be applied only to observational data, $\boldsymbol{f}$ indicates constraints on the function class of the SEM, ∂/∂ indicates differentiability, and the data column lists restrictions on the data distribution.

Method	$\mathbf{x}$	$do(\emptyset)$	$\boldsymbol{f}$	∂/∂	Data
Monti et al. (2019)	✗	✓	✓	✗	non-stationary
Shimizu et al. (2006)	✓	✓	linear	✗	non-Gaussian
Guo et al. (2022)	✓	✓	✓	✗	exchageability
Khemakhem et al. (2021)	✓	✓	affine/additive	✓	✓
Lachapelle et al. (2020)	✓	✓	additive	✓	Gaussian
Brouillard et al. (2020)	✓	✗	✓	✓	✓
Ke et al. (2020)	✓	✗	✓	✓	discrete
Lippe et al. (2021)	✓	✗	✓	✓	✓
Ng et al. (2022)	✓	✓	additive	✓	✓
Schölkopf et al. (2021)	✓	✓	linear/additive	✓	✓
Zheng et al. (2018)	✓	✓	linear	✓	✓
Yu et al. (2019)	✓	✓	additive	✓	✓
Shen et al. (2022)[6]	✓	✓	additive	✓	labeling
Kalainathan et al. (2018)	✓	✓	additive	✓	Gaussian
Rolland et al. (2022)	✓	✓	additive	✓	✓
Yang et al. (2021)[7]	✓	✓	additive	✓	labeling
Lorch et al. (2021)	✓	✓[8]	✓	✓	graph prior
Lorch et al. (2022)	✓	✓	✓	✓	graph prior
Charpentier et al. (2022)	✓	✓	✓	✓	graph prior
Zheng et al. (2022)	✓	✓	linear	✓	Gaussian
Squires et al. (2023)	✓	✗	linear	✗	✓
Atanackovic et al. (2023)	✓	✓	cyclic (ODE)	✓	✓
Ours	✓	✓	✓	✓	Assums. 2 and F.1

Table 5: Using the Jacobian in the literature for CD and/or identifiability. Column $\boldsymbol{f}$ indicates constraints on the function class of the SEM, the data column lists restrictions on the data distribution, $\mathbf{J}$ describes the Jacobian of which function is used, CD indicates use for causal discovery, and the identifiability column whether the method has identifiability guarantees.

Method	$\boldsymbol{f}$	Data	$\mathbf{J}$	CD	Identifiability
Shimizu et al. (2006)	linear	non-Gaussian	$\mathbf{J}_{\boldsymbol{f}^{-1}}$	✓	✓
Lachapelle et al. (2020)	additive	Gaussian	$\mathbf{J}_{\boldsymbol{f}^{-1}}$	✓	✗
Gresele et al. (2021)[9]	IMA[10]	✓	$\mathbf{J}_{\boldsymbol{f}}$	✗	✓
Zheng et al. (2022)	sparse	✓	$\mathbf{J}_{\boldsymbol{f}}$	✗	✓
Rolland et al. (2022)	additive	✓	score function	✓	✗
Atanackovic et al. (2023)	cyclic (ODE)	✓	$\mathbf{J}_{\boldsymbol{f}}$	✓	✗
Ours	✓	Assums. 2 and F.1	$\mathbf{J}_{\boldsymbol{f}^{-1}}$	✓	✓

E Proofs

E.1 Proof of Lem. 1

Lemma 1. *[DAG DGPs resolve the permutation ambiguity of ICA] When the DGP is a SEM with functional relationships $\boldsymbol{f}$ and an underlying DAG, then the permutation indeterminacy of ICA π_{ICA} can be accounted for such that the Jacobian of the inference network will have a lower-triangular Jacobian, even with unknown causal ordering π.*

Proof. The unknown causal ordering π of N_i implies the right-multiplication of $\mathbf{J}_{\boldsymbol{f}^{-1}}$ with π^{-1}, the permutation indeterminacy of ICA the left-multiplication with π_{ICA}, yielding the estimated Jacobian $\mathbf{J}_{\widehat{\boldsymbol{f}}^{-1}}$:

$$\mathbf{J}_{\widehat{\boldsymbol{f}}^{-1}} = \pi_{\text{ICA}} \circ \mathbf{J}_{\boldsymbol{f}^{-1}} \circ \pi^{-1}, \tag{23}$$

where π_{ICA} and π^{-1} are not necessarily the same.
If π is **unique**, we only need to show that π_{ICA} is also unique. Assume that there exists $\pi_{\text{ICA},1} \neq \pi_{\text{ICA},2}$ such that $\mathbf{J}_{\widehat{\boldsymbol{f}}^{-1}}$ can be transformed into a lower-triangular $\mathbf{J}_{\boldsymbol{f}^{-1}}$ by both. This implies that the rows of $\mathbf{J}_{\widehat{\boldsymbol{f}}^{-1}}$ can be permuted such that it yields a lower-triangular $\mathbf{J}_{\boldsymbol{f}^{-1}}$ (when π is already accounted for). Assume that $\pi_{\text{ICA},1}$ yields a lower-triangular $\mathbf{J}_{\boldsymbol{f}^{-1}}$. Then a different $\pi_{\text{ICA},2}$ means that there are at least two rows i, k in $\mathbf{J}_{\widehat{\boldsymbol{f}}^{-1}}$ that can be permuted differently than in $\pi_{\text{ICA},1}$ such that the resulting matrix is still lower-triangular. $\mathbf{J}_{\boldsymbol{f}^{-1}}$ has a non-zero diagonal (cf. the definition of $\mathbf{B}$ in (26)); thus, using a different ordering $\pi_{\text{ICA},2}$ will violate lower-triangularity, for this means that the ith, k^{th} rows after applying $\pi_{\text{ICA},1}$ will be equal to the kth, i^{th} rows of $\pi_{\text{ICA},2}$ (the former being equal to the true Jacobian $\mathbf{J}_{\boldsymbol{f}}$):

$$\left[\pi_{\text{ICA},1}^{-1} \circ \mathbf{J}_{\widehat{\boldsymbol{f}}^{-1}} \circ \pi\right]_{[i,k],:} = \left[\mathbf{J}_{\boldsymbol{f}^{-1}}\right]_{[i,k],:} = \left[\pi_{\text{ICA},2}^{-1} \circ \mathbf{J}_{\widehat{\boldsymbol{f}}^{-1}} \circ \pi\right]_{[k,i],:}, \tag{24}$$

which means that for $\pi_{\text{ICA},2}$ the resulting matrix has nonzero elements at indices (i, k) and (k, i). This violates lower-triangularity, since $k \neq i$, so one of the above means that there is at least one non-zero element above the main diagonal, leading to a contradiction.
If π is **not unique**, we can apply the above argument, resulting in a set of permutation matrices, each yielding a lower-triangular Jacobian. □

E.2 Proof of Prop. 1

Proposition 1. *[$\mathbf{J}_{\boldsymbol{f}^{-1}} \sim_{DAG} (\mathbf{I}_d - \boldsymbol{\mathcal{A}})$]The inverse DGP's Jacobian $\mathbf{J}_{\boldsymbol{f}^{-1}}$ is structurally equivalent to $(\mathbf{I}_d - \boldsymbol{\mathcal{A}})$, when Assum. 1 holds.*

[6]Supervised
[7]Supervised
[8]Lorch et al. (2021) can also leverage interventional data, but it also works from observations
[9]Gresele et al. (2021) proposed IMA and showed that it rules out spurious solutions; Buchholz et al. (2022) proved identifiability
[10]That is, $\mathbf{J}_{\boldsymbol{f}}$ has orthogonal columns

Proof. We start from the functional equation of the SEM and note that if $\boldsymbol{X}$ is the input of $\boldsymbol{f}$ (as $\boldsymbol{Pa}_i$ from (1)), then the output is the same $\boldsymbol{X}$ (which deterministically depends on $\boldsymbol{N}$):

$$\boldsymbol{X} = \boldsymbol{X}(\boldsymbol{N}) := \boldsymbol{f}(\boldsymbol{X}(\boldsymbol{N}), \boldsymbol{N}) = \boldsymbol{f}(\boldsymbol{X}, \boldsymbol{N}). \tag{25}$$

For a given $(\boldsymbol{X}, \boldsymbol{N})$ we can evaluate the Jacobian of $\boldsymbol{f}$ via the chain rule—the key point is that since $\boldsymbol{X}$ is a fix point of $\boldsymbol{f}$, $\mathbf{J}_{\boldsymbol{f}}$ will apprear on both sides (evaluated at the same point, expressed with the bar notation):

$$\mathbf{J}_{\boldsymbol{f}}\big|_{\boldsymbol{X},\boldsymbol{N}} = \tfrac{\partial \boldsymbol{X}(\boldsymbol{N})}{\partial \boldsymbol{N}}\big|_{\boldsymbol{X},\boldsymbol{N}} = \tfrac{\partial \boldsymbol{f}(\boldsymbol{X},\boldsymbol{N})}{\partial \boldsymbol{N}}\big|_{\boldsymbol{X},\boldsymbol{N}} = \mathbf{A}\tfrac{\partial \boldsymbol{X}}{\partial \boldsymbol{N}}\big|_{\boldsymbol{X},\boldsymbol{N}} + \mathbf{B} = \mathbf{A}\mathbf{J}_{\boldsymbol{f}}\big|_{\boldsymbol{X},\boldsymbol{N}} + \mathbf{B} \tag{26}$$

$$\mathbf{A} := \tfrac{\partial \boldsymbol{f}(\boldsymbol{X},\boldsymbol{N})}{\partial \boldsymbol{X}}\big|_{\boldsymbol{X},\boldsymbol{N}};\ \mathbf{B} := \tfrac{\partial \boldsymbol{f}(\boldsymbol{X},\boldsymbol{N})}{\partial \boldsymbol{N}}\big|_{\boldsymbol{X},\boldsymbol{N}}. \tag{27}$$

The above equation can be reordered to yield the expression for $\mathbf{J}_{\boldsymbol{f}}$ (note that $\mathbf{A}$, $\mathbf{B}$ depend on $\boldsymbol{X}$, $\boldsymbol{N}$):

$$\mathbf{J}_{\boldsymbol{f}}\big|_{\boldsymbol{X},\boldsymbol{N}} = (\mathbf{I}_d - \mathbf{A})^{-1}\mathbf{B}, \tag{28}$$

where $\mathbf{A}$ describes the $X_i - X_j$ edges in the DAG (i.e., $\mathbf{A} \sim_{DAG} \boldsymbol{\mathcal{A}}$), $\mathbf{B}$ is diagonal (as the $\boldsymbol{X}$ values are fixed). Since we reason about the Jacobian point-wise, we can invoke the inverse function theorem (by assumption, $\boldsymbol{f}$ is bijective) to express $\mathbf{J}_{\boldsymbol{f}^{-1}}$:

$$\mathbf{J}_{\boldsymbol{f}^{-1}} = \mathbf{J}_{\boldsymbol{f}}^{-1} = \mathbf{B}^{-1}(\mathbf{I}_d - \mathbf{A}). \tag{29}$$

$\mathbf{J}_{\boldsymbol{f}^{-1}} \sim_{DAG} (\mathbf{I}_d - \boldsymbol{\mathcal{A}})$ follows as $\mathbf{A} \sim_{DAG} \boldsymbol{\mathcal{A}}$ and $\mathbf{B}$ is diagonal (the invariance of $\sim_{DAG}$ follows from Def. 1(i)). □

Alternative proof

Proof. The proof consists of two steps: 1) leveraging the iterative formulation of the SEM (2), proving that $\mathbf{J}_{\boldsymbol{f}^{-1}} \sim_{DAG} (\mathbf{I}_d - \boldsymbol{\mathcal{A}})$ and 2) relying on the properties of $\sim_{DAG}$ and Lem. 1, showing $\mathbf{J}_{\boldsymbol{f}^{-1}} \sim_{DAG} \mathbf{J}_{\widehat{\boldsymbol{f}}^{-1}}$.
We start by formulating $\mathbf{J}_{\boldsymbol{f}}$ (recall that $\boldsymbol{X} = \boldsymbol{X}^d$) based on the iterative SEM expression (2):

$$\mathbf{J}_{\boldsymbol{f}}\big|_{\boldsymbol{X}^{d-1},\boldsymbol{N}} = \tfrac{\partial \boldsymbol{X}^d}{\partial \boldsymbol{N}}\big|_{\boldsymbol{X}^{d-1},\boldsymbol{N}} = \tfrac{\partial \boldsymbol{f}(\boldsymbol{X}^{d-1},\boldsymbol{N})}{\partial \boldsymbol{N}}\big|_{\boldsymbol{X}^{d-1},\boldsymbol{N}} = \mathbf{A}^{d-1}\tfrac{\partial \boldsymbol{X}^{d-1}}{\partial \boldsymbol{N}}\big|_{\boldsymbol{X}^{d-1},\boldsymbol{N}} + \mathbf{B}^{d-1} \tag{30}$$

$$\mathbf{A}^{d-1} := \tfrac{\partial \boldsymbol{f}(\boldsymbol{X}^{d-1},\boldsymbol{N})}{\partial \boldsymbol{X}^{d-1}}\big|_{\boldsymbol{X}^{d-1},\boldsymbol{N}};\ \mathbf{B}^{d-1} := \tfrac{\partial \boldsymbol{f}(\boldsymbol{X}^{d-1},\boldsymbol{N})}{\partial \boldsymbol{N}}\big|_{\boldsymbol{X}^{d-1},\boldsymbol{N}}, \tag{31}$$

where $\mathbf{A}$ describes the $X_i - X_j$ edges in the DAG (i.e., $\mathbf{A} \sim_{DAG} \boldsymbol{\mathcal{A}}$), $\mathbf{B}$ is diagonal (as the $\boldsymbol{X}^{d-1}$ values are fixed). Although both $\mathbf{A}, \mathbf{B}$ are dependent from t (superscript), unless $\boldsymbol{f}$ is linear, they are independent when seen through the lens of structural equivalence. By Assum. A.1, it holds that $\mathbf{A}^k \sim_{DAG} \mathbf{A}^j \wedge \mathbf{B}^k \sim_{DAG} \mathbf{B}^j : \forall j, k$. Thus, we will omit superscripts for both.
Realizing that (30) gives us a recursive formula, and recalling that $\boldsymbol{X}^0 = \mathbf{0}$, we can unroll (30) iteratively for $t = d-1, d-2, \ldots, 0$:

$$\mathbf{J}_{\boldsymbol{f}} = \mathbf{A}\tfrac{\partial \boldsymbol{X}^{d-1}}{\partial \boldsymbol{N}} + \mathbf{B} \sim_{DAG} \mathbf{A}\left[\mathbf{A}\tfrac{\partial \boldsymbol{X}^{d-2}}{\partial \boldsymbol{N}} + \mathbf{B}\right] + \mathbf{B} \sim_{DAG} \mathbf{A}\left[\mathbf{A}\left[\ldots\left[\mathbf{A}\underbrace{\tfrac{\partial \boldsymbol{X}^0}{\partial \boldsymbol{N}}}_{=\mathbf{0}} + \mathbf{B}\right]\right] + \mathbf{B}\right] + \mathbf{B} \tag{32}$$

$$= \sum_{i=0}^{d-1} \mathbf{A}^i \mathbf{B} = (\mathbf{I}_d - \mathbf{A})^{-1}\mathbf{B}, \tag{33}$$

where the structural equivalences follow by the structural faithfulness of $\mathbf{J}_{\boldsymbol{f}}$ (Assum. A.1), the last equality expresses the sum of the geometric series with elements $\mathbf{A}^i$ (the sum is finite as $\mathbf{A}$ is strictly lower triangular). By invoking the inverse function theorem (by assumption, $\boldsymbol{f}$ is bojective), we can express $\mathbf{J}_{\boldsymbol{f}^{-1}}$:

$$\mathbf{J}_{\boldsymbol{f}^{-1}} = \mathbf{J}_{\boldsymbol{f}}^{-1} \sim_{DAG} \mathbf{B}^{-1}(\mathbf{I}_d - \mathbf{A}). \tag{34}$$

$\mathbf{J}_{\boldsymbol{f}^{-1}} \sim_{DAG} (\mathbf{I}_d - \boldsymbol{\mathcal{A}})$ follows as $\mathbf{A} \sim_{DAG} \boldsymbol{\mathcal{A}}$ and $\mathbf{B}$ is diagonal (the invariance of $\sim_{DAG}$ follows from Def. 1(i)). □

F NLICA with Contrastive Learning

Assumption F.1 (Contrastive model on $\mathbb{R}^d$)**.** *We assume that the model satisfies the following conditions:*

(i) The encoder is defined as $\widehat{\boldsymbol{f}}^{-1} : \mathcal{X} \to \mathcal{N}'$, where $\mathcal{N}' \subseteq \mathbb{R}^d$ is a convex body (hyperrectangle);

(ii) The conditional distribution $q(\widetilde{\boldsymbol{N}}|\boldsymbol{N})$ associated with our model $\widehat{\boldsymbol{f}}^{-1}$ through $\boldsymbol{h} = \widehat{\boldsymbol{f}}^{-1} \circ \boldsymbol{f}$ is given by $q(\widetilde{\boldsymbol{N}}|\boldsymbol{N}) = C_q^{-1}(\boldsymbol{N}) e^{-\left|\boldsymbol{h}(\widetilde{\boldsymbol{N}})-\boldsymbol{h}(\boldsymbol{N})\right|/\boldsymbol{\tau}}$ with $C_q(\boldsymbol{N}) := \int e^{-\left|\boldsymbol{h}(\widetilde{\boldsymbol{N}})-\boldsymbol{h}(\boldsymbol{N})\right|/\boldsymbol{\tau}} d\widetilde{\boldsymbol{N}}$, where $C_q(\boldsymbol{N})$ is the partition function, $\boldsymbol{\tau} > 0$ is a scale parameter, and δ is the semi-metric from Assum. 2.

(iii) The encoder is trained with a contrastive loss $\mathcal{L}_{\text{CL}}$ using the same L_1 metric, i.e.,

$$\mathbb{E}_{(\boldsymbol{X},\widetilde{\boldsymbol{X}},\boldsymbol{X}^-)}\left[-\log \frac{\exp\left[-\left|\widehat{\boldsymbol{f}}^{-1}(\boldsymbol{X}) - \widehat{\boldsymbol{f}}^{-1}(\widetilde{\boldsymbol{X}})\right|/\boldsymbol{\tau}\right]}{\exp\left[-\left|\widehat{\boldsymbol{f}}^{-1}(\boldsymbol{X}) - \widehat{\boldsymbol{f}}^{-1}(\widetilde{\boldsymbol{X}})\right|/\boldsymbol{\tau}\right] + \sum_i^M \exp\left[-\left|\widehat{\boldsymbol{f}}^{-1}(\boldsymbol{X}^-) - \widehat{\boldsymbol{f}}^{-1}(\widetilde{\boldsymbol{X}})\right|/\boldsymbol{\tau}\right]}\right], \quad (35)$$

where $\widetilde{\boldsymbol{X}}$ is the positive pair, $\boldsymbol{X}^-$ are the negative pairs, and M is the number of negative pairs;

(iv) During training one has access to observations $\boldsymbol{X}$, which are samples from these distributions transformed by the generator function (i.e., the SEM) $\boldsymbol{f}$.

Are the distributional assumptions for contrastive NLICA testable for CD? The assumptions on the conditional $p(\widetilde{\boldsymbol{N}}|\boldsymbol{N})$ and marginal $p(\boldsymbol{N})$ distributions (Assum. 2) for contrastive NLICA might be deemed peculiar in the context of CL. First, we emphasize that since our results do not require the use of contrastive NLICA, the user is free to chose a different method that guarantees strong identifiability. However, if contrastive NLICA is deemed suitable for a task, then

1. they are neither interfering with assumptions in CD; and
2. they are testable—e.g., by a one-sample Kolmogorov-Smirnov test (Kolmogorov, 1933; Smirnov, 1948).

What we mean by the first point (and elucidate in the next section) that to fulfill Assum. 2, we neither leave nor constrain the function class of $\boldsymbol{f}$.

G Experimental details

Table 6: Hyperparameters for our experiments (§ 5)

Parameter	Values
$\widehat{\boldsymbol{f}}^{-1}$	6-layer MLP
Activation	Leaky ReLU
Batch size	6144
Learning rate	1e−4
$\mathbb{R}^d$	$[0;1]^d$
C_p	1
m_p	0
C_{param}	0.05
m_{param}	1
p	1
$\boldsymbol{\tau}$ (in $\mathcal{L}_{\text{CL}}$)	1
α	0.5

Table 7: Results for **sparse** linear and nonlinear SEMs. Mean Correlation Coefficient (MCC) measures identifiability, $|\mathcal{E}^*|$ is the maximum number of edges in a DAG, Acc is accuracy, Ours is our proposal, HSIC refers to using HSIC independence tests, and SHD is the Structural Hamming Distance

		Linear				Nonlinear			
$\lvert\mathcal{E}^*\rvert$	d	MCC	Acc(Ours)	Acc(HSIC)	SHD	MCC	Acc(Ours)	Acc(HSIC)	SHD
6	3	1.	$0.917_{\pm 0.108}$	$0.708_{\pm 0.11}$	0.111	1.	$0.889_{\pm 0.111}$	$0.75_{\pm 0.144}$	0.111
15	5	$0.961_{\pm 0.062}$	$0.768_{\pm 0.121}$	$0.784_{\pm 0.111}$	$0.256_{\pm 0.132}$	$0.972_{\pm 0.059}$	$0.76_{\pm 0.095}$	$0.84_{\pm 0.098}$	$0.208_{\pm 0.0873}$
36	8	$0.844_{\pm 0.184}$	$0.709_{\pm 0.084}$	$0.711_{\pm 0.122}$	$0.322_{\pm 0.109}$	$0.783_{\pm 0.155}$	$0.656_{\pm 0.059}$	$0.708_{\pm 0.119}$	$0.375_{\pm 0.081}$
55	10	$0.8_{\pm 0.217}$	$0.648_{\pm 0.059}$	$0.715_{\pm 0.1}$	$0.336_{\pm 0.055}$	$0.734_{\pm 0.206}$	$0.618_{\pm 0.044}$	$0.69_{\pm 0.086}$	$0.37_{\pm 0.082}$

Table 8: Results for **permuted** (i.e., π is not the identity) linear and nonlinear SEMs. Mean Correlation Coefficient (MCC) measures identifiability, $|\mathcal{E}^*|$ is the maximum number of edges in a DAG, Acc is accuracy, Ours is our proposal, HSIC refers to using HSIC independence tests, and SHD is the Structural Hamming Distance

		Linear				Nonlinear			
$\lvert\mathcal{E}^*\rvert$	d	MCC	Acc(Ours)	Acc(HSIC)	SHD	MCC	Acc(Ours)	Acc(HSIC)	SHD
6	3	1.	1.	0.667	0.	1.	1.	0.667	0.
15	5	$0.989_{\pm 0.039}$	$0.949_{\pm 0.098}$	$0.866_{\pm 0.088}$	$0.051_{\pm 0.098}$	$0.988_{\pm 0.039}$	$0.94_{\pm 0.087}$	0.863	$0.06_{\pm 0.087}$
36	8	$0.837_{\pm 0.252}$	$0.834_{\pm 0.162}$	$0.624_{\pm 0.127}$	$0.166_{\pm 0.162}$	$0.752_{\pm 0.232}$	$0.794_{\pm 0.138}$	$0.687_{\pm 0.139}$	$0.206_{\pm 0.138}$
55	10	$0.852_{\pm 0.251}$	$0.761_{\pm 0.213}$	$0.578_{\pm 0.086}$	$0.239_{\pm 0.213}$	$0.794_{\pm 0.255}$	$0.705_{\pm 0.16}$	$0.573_{\pm 0.05}$	$0.295_{\pm 0.159}$

G.1 Code for the Sinkhorn operator

```python
import torch
from torch import nn as nn


class SinkhornOperator(object):
    """
    Based on http://arxiv.org/abs/1802.08665
    """

    def __init__(self, num_steps: int):

        if num_steps < 1:
            raise ValueError(f"{num_steps=} should be at least 1")

        self.num_steps = num_steps

    def __call__(self, matrix: torch.Tensor) -> torch.Tensor:
        def _normalize_row(matrix: torch.Tensor) -> torch.Tensor:
            return matrix - torch.logsumexp(matrix, 1, keepdim=True)

        def _normalize_column(matrix: torch.Tensor) -> torch.Tensor:
            return matrix - torch.logsumexp(matrix, 0, keepdim=True)

        S = matrix

        for _ in range(self.num_steps):
            S = _normalize_column(_normalize_row(S))

        return torch.exp(S)
```

Figure 10: PyTorch code for implementing the Sinkhorn operator from (Mena et al., 2018). A Sinklhorn network applies `SinkhornOperator` to the scaled weight matrix $\mathbf{W}/\boldsymbol{\tau}$, where $\boldsymbol{\tau}$ is generally around $1 \cdot 10^{-3}$.

H Notation

Acronyms

IMA Independent Mechanism Analysis

ANM Additive Noise Model

CD Causal Discovery
CdF Causal de Finetti
CL Contrastive Learning

DAG Directed Acyclic Graph
DGP Data Generating Process

i.i.d. independent and identically distributed
ICA Independent Component Analysis
ICM Independent Causal Mechanisms

LiNGAM Linear Non-Gaussian Acyclic Model
LSTM Long Short-Term Memory

MCC Mean Correlation Coefficient
MLP Multi-Layer Perceptron

NLICA nonlinear Independent Component Analysis

ODE Ordinary Differential Equation

SEM Structural Equation Model
SHD Structural Hamming Distance

Nomenclature

$\mathcal{L}_\pi$ regularizer for learning π
$\mathbf{S}$ Sinkhorn network
$\mathcal{E}$ edge set of a graph
$\mathcal{L}$ loss function
$\boldsymbol{h}$ composition of encoder and decoder
d problem dimensionality

Algebra

α scalar field
$\mathbf{D}$ diagonal matrix
$\mathbf{I}_d$ d-dimensional identity matrix
$\mathbf{J}$ Jacobian matrix
$\mathbf{P}$ permutation matrix

Causality

N noise (independent) variable component
X observation component
$\boldsymbol{N}$ noise (independent) variable vector
$\boldsymbol{Pa}$ parent set of $\boldsymbol{X}$
$\boldsymbol{X}$ observation vector
$\boldsymbol{\mathcal{A}}$ adjacency matrix of a SEMs
$\boldsymbol{\mathcal{C}}$ connectivity matrix of a SEMs
$\boldsymbol{f}$ structural assignment in SEMs
$\mathcal{I}$ index set
$\mathcal{N}$ space of the noise variables
$\mathcal{X}$ space of the effect variables
π causal ordering
$\sim_{DAG}$ structural equivalence
f a component of $\boldsymbol{f}$

Contrastive Learning

M number of negative samples
$\mathcal{L}_{\text{CL}}$ contrastive loss function
$\widetilde{\boldsymbol{N}}$ positive latent vector
$\widetilde{\boldsymbol{X}}$ positive observation vector
$\boldsymbol{X}^-$ negative observation vector
$\boldsymbol{\tau}$ temperature in $\mathcal{L}_{\text{CL}}$